# *Electrochemical reduction and simultaneous N-doping of nanographene oxide in acetonitrile for DNA-selective biosensors*


Student: Emily Kathryn Kemp, 38970, ekemp@abo.fi

Home institution: Master of Science, Chemistry
Laboratory of Analytical Chemistry
Faculty of Science and Engineering
Åbo Akademi University
Åbo, Finland

Supervisor: Dr. Zhanna Boeva

Master's Thesis 2019

# Table of Contents

# Abbreviations

| | |
|---|---|
| ACN | Acetonitrile |
| AO | Ascorbic oxidase |
| BSA | Bovine serum albumin |
| cDNA | Complementary DNA |
| CT-DNA | Calf thymus DNA |
| CV | Cyclic voltammetry |
| CVD | Chemical vapour deposition |
| dsDNA | Double stranded DNA |
| EDOT | 3,4-Ethylenedioxythiophene |
| EDTA | Ethylenediaminetetraacetic acid |
| EIS | Electrochemical impedance spectroscopy |
| GC | Glassy carbon |
| GCE | Glassy carbon electrode |
| GO | Graphene oxide |
| ncDNA | non-complementary DNA |
| nGO | Nanographene oxide |
| NGO | Nitrogen-doped graphene oxide |
| OCP | Open circuit potential |
| PBS | Phosphate buffered saline |
| PPyox | Oxidized polypyrrole |
| RGO | Reduced graphene oxide |
| RnGO | Reduced nanographene oxide |
| RNGO | Reduced and N-doped graphene oxide |
| RNnGO | Reduced and N-doped nanographene oxide |
| SDS | sodium dodecyl sulfate |
| SEM | Scanning electron microscopy |
| SSC | Saline sodium citrate |
| ssDNA | Single stranded DNA |
| SWCNT | Single-walled carbon nanotubes |

# Abstract

Graphene and its derivatives have been a focus of research for a number of years due to their enhanced surface area and electrical conductivity making them a viable candidate for electrochemical sensing. Previously, the preparatory method for a DNA-selective biosensor based on electrochemically reduced and N-doped nanographene oxide (RNnGO) displayed a high degree of irreproducibility, low target DNA detection rates and minimal signal response. The objective of this work was, therefore, to prepare RNnGO to be further used in an electrochemical biosensor that would improve sensor reproducibility as well as the selective detection of target DNA. The drop-casting method was used to modify glassy carbon electrodes with a film of nanographene oxide (nGO) where maximum surface coverage was determined to be reached with 17 5-μL aliquots of nGO in aqueous solution cast to the electrode surface followed by annealing for 1 hour at 60°C. Characterization by scanning electron microscopy showed that the annealing process aided in the evaporation of remaining aqueous solution resulting in increased surface roughness compared to not annealed nGO. The optimized drop-casting method greatly minimized deviations between electrodes as well as increased the charge capacity of the RNnGO films. The nGO films were reduced in the presence of acetonitrile in order for N-doping of the material to occur. The resulting RNnGO films were characterized by cyclic voltammetry and electrochemical impedance spectroscopy and compared to reduced nGO in order to determine the effects of N-doping on the material's electrochemical properties. The introduction of N-atoms resulted in a slightly negative charge of the surface and a higher conductivity. For use as DNA-selective biosensor, single-stranded probe DNA was immobilized on the surface using crosslinking chemistry via the primary amine groups present in the surface and the thiol groups present at one end of the DNA probe. Areas left bare by a lack of N-atoms available for DNA probe immobilization were best blocked by calf-thymus DNA due to its length and flexibility allowing for a high conformity to the surface. Target DNA in the sample was detected by cyclic voltammetry after hybridization with probe DNA via charge transfer of $[Ru(NH_3)_6]^{3+}$ cations intercalated within the negatively charged DNA backbone. The window of potentials for reduction and N-doping of nGO was varied in order to identify the potential window that resulted in the highest signal amplification and rate of successful detection of target DNA. An applied reduction potential of -2.215 V was found to provide the optimum degree of N-doping which resulting in a 69% increase in surface charge after immobilization of the DNA probe, analogous to an increase in DNA surface density. DNA-selective sensors prepared using these experimental methods resulted in a successful target DNA detection rate of 100% and an increase in positive signal amplitude by a factor of 1.5.

# 1. Introduction

Often, electrochemical techniques are underestimated in their ability to perform analysis to the same level of accuracy and precision as other analytical techniques. Electrochemistry, however, has proven to be fast, cost effective and simple while still being sensitive and selective. In fact, it boasts several advantages over techniques used in well-equipped laboratories such as the possibility of integration into miniature devices for fast and reliable analysis.

The detection of a specific strand of DNA can be invaluable to the diagnosis of genetic diseases. For example, detecting circulating tumor DNA even before the cancerous tumour has become detectable by other methods. Generally, DNA sequencing is done by special sequencing instruments that determine the order of base pairs within a strand of DNA. Electrochemically, however, a positive or negative signal can be obtained for a specific strand of DNA by taking advantage of the tendency for single-stranded DNA to hybridize (to form a double strand) with its complementary strand immobilized at the surface of an electrode and serving as a probe for biosensing. By immobilizing a specific sequence of DNA to the surface, the electrode can be tailored to detect its complementary DNA in the sample. In the further advancement of the technology one can utilize, for example, silicon microchips for immobilization of hundreds and thousands of DNA molecules and creating this way multielectrode array for high throughput electrochemical detection of various fragments of DNA via hybridization events.

The electrochemical detection of DNA suffers from one general drawback: the low detected currents recorded after hybridization event making thus the method lagging behind fluorescent techniques. Therefore the enhancement of the electrochemical response is very much desired. This is typically done through modification of the electrode surface with various materials capable to amplify current by enhancement of the electron transfer at the electrode surface. One such material is considered to be graphene and its derivatives.

Graphene has been acclaimed for its increased electrical conductivity and electroactive surface area compared to other materials. Its limitations, however, include difficulties in mass production due to its 2D structure. Derivatives of graphene are therefore considered viable alternatives that are more accessible but that still boast the same advantages. One such material is graphene oxide (**GO**) which, while non conducting itself, can be reduced in order to remove the oxygen-containing groups, which give it its insulating properties, and consequently restore its electrical conductivity. Methods for reduction include thermal or chemical reduction of GO, however, these methods involve high temperatures and hazardous chemicals. In comparison, electrochemical methods are a promising alternative approach for the reduction of GO due to their safer approach and

the possibility to tailor the electrochemical properties of the reduced GO film. To further increase material conductivity, dopant molecules can be introduced to the graphene oxide film (Ambrosi *et al.*, 2016) which either provide electrons, as an electron donor, or holes, as an electron acceptor. Nitrogen is effective as an electron donor and is often used as a dopant in graphene derivatives reinforcing their enhanced electrocatalytic properties. Additionally, nitrogen-containing groups inserted to the graphene structure enable further modification of the surface with biomolecules for potential use as a biosensor. N-doping can be performed by methods such as chemical vapour deposition, thermal annealing and plasma treatment, however, similar to the reduction of GO, they involve hazardous chemicals and high temperatures. It is therefore beneficial to consider electrochemical methods for the simultaneous reduction and N-doping of GO.

Reduction and N-doping of GO has been achieved previously by applying a cathodic potential window to an electrode in the presence of an aqueous solution containing GO and ammonia. The negative potential simultaneously reduces and N-dopes GO as it is deposited at the electrode surface (Ma *et al.,* 2015). An alternate method is to initially dropcast GO on the electrode surface followed by reduction of the oxygen-containing groups in the presence of a nitrogen containing solution in order to promote N-doping. This method, however, shows irreproducibility of the reduction and N-doping of GO between electrodes. In order to reduce error, the drop-casting of nanographene oxide (**nGO**) therefore requires optimization in order to obtain complete surface coverage of the electrode. Furthermore, the tailoring of the electrochemical properties of the resulting reduced and N-doped nanographene oxide (**RNnGO**) film has to be carefully considered when taking into account the application of the material in a DNA biosensor.

The current work will focus on the optimization of the preparatory methods used for RNnGO modified electrode with a direct application in a DNA selective biosensor. The initial drop-casting technique used to deposit nGO will be improved in order to attain a reproducible and complete surface coverage of the electrode surface. Secondly, identification of the optimum reduction potential window will be necessary to tailor the extent of reduction and N-doping of nGO for the subsequent immobilization of the DNA probe. Finally, the resulting modified electrodes will be tested for the selectivity for target DNA by performing cyclic voltammetry in the presence of the redox cation $[Ru(NH_3)_6]^{3+}$ routinely used for detection of DNA hybridization in scientific community.

# 2. Literature Overview

## Graphene

When graphene was isolated from graphite, its unique physical and chemical properties quickly gained interest from researchers around the world. These graphene films consist of carbon atoms in a 2-dimensional, benzene-ring pattern whose layers can be peeled apart to obtain one atom thick sheets (Novoselov and Geim *et al*., 2004). In solids, the electrons in the highest occupied energy levels are said to be in the valence band while the lowest unoccupied energy levels make up the conduction band. The difference in these energy levels is called bandgap and is the largest for insulators and the smallest in metals. In the case of graphene, the valence band and the conduction band overlap. Each carbon atom has σ-bonds with its three neighbours and a p-orbital containing a valence electron which is perpendicular to the lattice plain. Each carbon atom's p-orbital is hybridized with its neighbours' to form a π-bond which extends over the entire lattice surface forming bands. This means that the valence electrons can move freely through the conduction band with less energy dissipation, which accounts for the increased conductivity compared to other metals such as copper (Novoselov and Geim *et al*., 2004). Other advantages are that it is light, transparent and flexible while being the strongest material discovered to date.

The applications for graphene have extended to all areas of research including electronics for conductive displays and inks (Zhu *et al.*, 2011, Torrisi *et al*., 2012). It is used in filtration membranes as a barrier to unfavourable molecules and atoms in liquids and gasses (Cohen-Tanugi *et al.*, 2012, Jiang *et al.*, 2009). There are also advantages in combining graphene with existing materials often used in athletics and aerospace. Epoxy polymers, found in equipment ranging from tennis racquets to aircraft rudders, functionalized with graphene have been shown to have increased resistance to fracture and fatigue (Rafiee *et al*., 2009). The possibilities for graphene incorporated into micrometer-sized sensors used to detect the presence of harmful chemicals in food-packaging or in a larger-scale environment have also been explored (Sundramoorthy *et al.*, 2018). Equally as promising are graphene's potential benefits to biomedicine at the nano-level. Graphene has been used to modify

drugs to aid in targeted drug delivery. This includes modifying originally water insoluble anticancer drugs with graphene to obtain higher efficacy and water solubility of the drug (Liu *et al*., 2008).

The properties of graphene make it a prime candidate for applications in electrochemistry and studies employing electroactive species. It can be modified into various graphene derivatives such as graphene oxide or doped graphene which contain species that will either gain electrons and be reduced or lose electrons and be oxidized. This transfer of electrons, between the graphene-based element and electroactive analytes contained in the electrochemical cell, results in the completion of an electrical circuit and a measurable output signal. Graphene, in various forms, has been successfully used to modify electrodes and enhance their electrochemical properties. The advantage of graphene over other electrically conducting materials is that electrons that flow through the material do so with zero rest mass. This means that they can travel an infinite range rather than being limited by a finite mass (Dubonos *et al.*, 2005). Furthermore, electron transfer between redox species and the graphene-based material can be enhanced owing to the increased surface area, electrical conductivity and any modifications that optimize electrode affinity to a specific analyte (Geim *et al.,* 2007, Ambrosi *et al*., 2016). This, in turn, opens up possibilities for higher sensitivity and selectivity in electrochemical measurements.

## Graphene oxide and its reduction

While graphene itself exhibits many advantageous properties, it is difficult to mass-produce due to its 2D structure. Therefore, researchers have found many different ways to attain graphene-based products from graphite. Such materials include graphene oxide (**GO**), which is most often prepared using the Hummers, or modified Hummers, method (Hummers and Offeman, 1958). Typically, graphite is treated with sulfuric acid, sodium nitrate and potassium permanganate to oxidise graphite and thus introduce negatively charged groups to individual sheets of graphene. The charge repulsion will facilitate exfoliation of graphene oxide which yields single layers of few-atom thick sheets separated from each other. GO is characterized by its oxygen-containing functional groups, which renders it hydrophilic and accounts for its conductive properties. In the oxidised form the polyconjugated system of π-bonds is disrupted with oxygen containing groups. Due to the extent

of the oxidation usually being high for preparative purposes, GO is therefore an insulator. In order to regain electrical conductivity, the functional groups can be removed through the reduction of GO either thermally, chemically or electrochemically (Park *et al.*, 2009). Thermal reduction involves rapidly heating GO to 1050°C which causes the oxygen-containing groups to decompose into gases and expand (Schniepp *et al.*, 2006). The result are single sheets of graphene functionalized with oxygen-containing groups. The chemical reduction of GO can be achieved by combining GO and hydrazine hydrate at 100°C (Stankovich *et al.*, 2007). While thermal and chemical reduction give efficient and high quality graphene, they include downsides such as high temperatures, hazardous reducing agents and the requirement of special equipment. Alternatively, electrochemical methods to reduce GO not only eliminate these previous drawbacks but bring further advantages to the use of graphene in experimental research and industrial applications. The electrochemical reduction of GO is most often performed by linear sweep voltammetry which provides a simple yet effective method that can be tailored to fit a multitude of experimental conditions (Dreyer *et al.*, 2010). By employing cyclic voltammetry as the reduction method, it is possible to observe the increase in measured current as the functional groups of GO are reduced and electrical conductivity increases. When the redox peaks reach a maximum, the reduction is considered complete, however, this method also enables the possibility to observe and control the extent of reduction as the process occurs.

One such electrochemical method is to deposit GO on a desired substrate, insulating or conductive, by spray-coating and subsequently reducing it by linear sweep voltammetry in sodium phosphate buffer (Zhou *et al.*, 2009). This combination provides an opportunity to tailor the thickness and pattern of the spray-coated film and reduce it using an environmentally friendly electrolyte solution. Through XPS analysis, the O/C ratio was found to be 4.23% compared to 6.25% which was initially determined to be the theoretical limit of oxygen reduction in GO (Boukhvalov *et al.*, 2008). The electrical conductivity of the films was measured at eight orders of magnitude larger than the initial GO which indicates the capability of this method to reinstate the system of π-bonds critical to the films' electrical conductivity. In addition to a superior GO reduction, the application of this method showed potential for the development of intricate electronic devices which require controlled thicknesses, patterns and flexibility in the physical and conductive properties of the substrate used.

Another such method involves GO deposition by drop-casting and reduction by performing cyclic voltammetry from -0.9 to 0 V (*vs* Hg/HgO) in 6 M potassium hydroxide (Zhang *et al.*, 2012). Contrary to alternate approaches, the GO reduction was considered to be largely successful with an O/C ratio of 1.29% determined by XPS. The capacitance of the reduced graphene oxide (**RGO**) films was also measured to be 152 F $g^{-1}$ and demonstrated stability over a period of 3000 charge/discharge cycles. This distinguishes it as a potential electrode material in electrical double layer capacitors as well as supercapacitors, which require high surface area and stability for superior capacitive properties and long cycle life.

Finally, GO reduced by cyclic voltammetry from -1.0 to 0.1 V (*vs* reversible hydrogen electrode) in 0.1 M $Na_2SO_4$ contain a certain percentage of quinone functional groups which are known to catalyze the reduction of $O_2$ and $H_2O_2$ better than other materials (Shao *et al.,* 2010). $O_2$ is required as an oxidant to enable the conversion of a chemical reaction to electricity in a fuel cell while $H_2O_2$ is a product of various enzymatic reactions. The use of RGO as an electrocatalyst in redox reactions requiring these molecules, therefore, has the potential to improve existing applications in fuel cells and biosensors.

## N-doping

While reducing GO restores its electrical conductivity, the specific electrical and optical properties of graphene can be modified further by the addition of dopants; molecules introduced to the graphene structure that are either electron acceptors, type p-doping, or electron donors, type n-doping. The addition of these molecules creates a new energy level between the conduction and valence bands, forming a band gap between the once overlapping energy levels of graphene. By performing p-type doping, the energy level of the electron acceptor will be closer to the valence band, resulting in the possibility of graphene's valence electrons to be easily excited to the new energy level and leaving holes in the valence band. In contrast, n-type doping creates an energy level close to the conduction band where the donor's electrons can be thermally excited into graphene's conduction band. In both cases, the addition of these dopants can greatly improve the conductivity of the material (Wei *et al.,* 2010). This renders doped graphene suitable as a (semi)conductor for many purposes

such as fuel cells (Qu *et al.*, 2010), field effect transistors (Kwon *et al.*, 2012), capacitors (Seredych *et al.*, 2008), and biosensors (Shao *et al.,* 2010).

Doping of graphene can either be done by interstitial doping, where dopants are adsorbed to the surface, or by substitutional doping, where carbon atoms within the graphene structure are replaced by dopants. Interstitial doping can be attained by simply exposing graphene to the desired dopant. Methods for interstitial doping using gaseous substances such as $H_2O$ or $NH_3$ (Novoselov and Geim *et al*., 2004), metals such as Co, Ni and Pd (Giovannetti *et al.*, 2008) as well as organic molecules such as tetrafluoro-tetracyanoquinodimethane (Chen *et al.*, 2007) have all been proven to modify the electrical properties of graphene.

The most common atoms used as dopants in substitutional doping include boron, sulfur, nitrogen and phosphorous. Nitrogen is of particular interest since it has been shown that, when used as a dopant in graphene, it affects the spin density and atomic charge distribution of the neighbouring carbon atoms. Compared to pristine graphene, where the spin and charge density is uniformly distributed, the addition of N atoms results in certain carbon atoms becoming electrochemically active (Zhang *et al.*, 2011). N atoms are introduced to the graphene structure with various bonding configurations. Pyridinic N is bound within a hexagonal ring and provides one p electron, pyrrolic N provides two p electrons and is bound into five-membered ring, and quaternary N replaces a carbon atom within the hexagonal ring and can be bound to three carbon atoms. Methods for substitutional doping of graphene with nitrogen include chemical vapour deposition (**CVD**), solvothermal approach, arc discharge method, thermal annealing and plasma treatment. A technique using CVD grows N-doped graphene by using a flow of $NH_3$ and $CH_4$ over a catalytic substrate at high temperatures (Wei *et al.*, 2009). The reaction of $CCl_4$ and $Li_3N$ can be employed to produce N-doped graphene using the solvothermal method (Deng *et al.*, 2011). High quality graphene containing 4.92% N was attained using the arc discharge method with flake graphite and melamine as the carbon and nitrogen source respectively as well as a catalyst such as ZnO or ZnS (Huang *et al.*, 2013). Through thermal annealing, GO can be reduced and N-doped in the presence of $NH_3$ at temperatures from 300 – 500°C to produce reduced and N-doped GO (**RNGO**) with N contents as high as 5% (Li *et al.*,

2009). Finally, graphene can be treated by nitrogen plasma where the percentage of N-doping is dependent on time (Wang *et al.*, 2010).

Similar to the aforementioned reduction of GO, these methods for the N-doping of graphene include the same downsides of harmful chemicals and high temperatures. Electrochemical methods are, therefore, a promising alternative. Nitrogen-doped graphene oxide (**NGO**) has been attained by cyclic voltammetry **(CV**) in $NH_4Cl/NH_3{\cdot}H_2O$. By cycling over a cathodic potential window of -0.8 to -1.6 V (*vs* Ag/AgCl), the oxygen-containing functional groups are removed leaving active carbon sites available for reacting with nitrogen-containing species (Ma *et al.*, 2015). It has also been shown that sheets of N-doped graphene can be achieved through anodic exfoliation (Yang *et al.*, 2016). Here, a constant potential of 10 V is applied between the anode, graphite, and an inert cathode in an electrochemical cell containing a glycine ammonia solution. Due to the high voltage, water is oxidized forming hydroxyl and oxygen radicals which in turn modify the edges of the graphite anode with -COOH and -OH functional groups. This oxidation process results in the introduction of glycine anions from the electrolyte solution as the graphite edges start to separate. A second oxidation of glycine anions produces $H_2NCH_2^+$ which, through amidation, forms $H_2NCH_2CONHCH_2^-$ and eventually results in $H_2NCH_2[CONHCH_2]_n^-$ by electropolymerization causing swelling and expansion of graphite. Nitrogen atoms are introduced to the graphite layers as a product of the oxidation of ammonia by the oxygen-containing functional groups (Lomosco *et al.,* 2011). Exfoliation of N-doped graphene sheets is caused by the carbonization of $H_2NCH_2CONHCH_2^-$ as well as from the production of $O_2$ and $CO_2$ gases in the initial oxidation step of the graphite anode.

## Biosensing

A biosensor is a sensing device modified with a biomolecule that is able to detect the presence of specific analyte (Turner *et al.,* 1987). The physicochemical signal produced from the biorecognition event between the biomolecule and the analyte is converted into an electrical signal by the sensor transducer and is proportional to the concentration of analyte present. Signal transduction methods include optical, thermometric, piezoelectric and electrochemical. Optical biosensors are based on the interaction of light with the biomolecule; one that either itself emits a

measurable signal upon reacting with the analyte or that contains a label that emits a signal. The range of measurable optical signals include the refractive index, fluorescence, absorbance and emission of light. In other cases, the reaction between the sensing biomolecule and the analyte is exothermic where heat is one of the products. This measurable change in temperature is the basis for thermometric sensors. Piezoelectric biosensors are based on a piezoelectric crystal, modified with a known amount of biomolecule, that oscillates at a given frequency when a potential is applied. As the biomolecule specifically binds the analyte, the mass of the crystal changes which in turn changes its vibrational frequency. The change in measured output signal can be related back to the mass of analyte bound to the surface of the sensor. Finally, a variety of electrochemical biosensors exist that measure changes in different electrical signals which occur when the biomolecule reacts with the analyte. An amperometric biosensor uses an applied potential to evoke reduction and oxidation of the species present and measures the change in current. Potentiometric sensors, however, measure the potential difference between a reference electrode and the working electrode where the biorecognition event takes place. Another method is to use electrochemical impedance spectroscopy to determine the impedance, specifically the resistance and capacitance, of the sensor components where any changes are related to the analyte binding to the biomolecule. In the case of conductometric biosensors, a potential is applied across two separate electrodes within an electrochemical cell and the resulting current flow between them is measured. As the result of the biorecognition event, the concentration of ionic species changes which in turn affects the conductivity of the cell solution and the current flow. As such, electrochemical biosensors provide a large degree of versatility and applicability when it comes to the wide range of biomolecular interactions possible. Compared to other methods of analysis, such as mass spectrometry or chromatography, the sample preparation for electrochemical analysis is easy and less time consuming. The required instrumentation is simple and inexpensive which creates the opportunity for miniaturization into portable devices making them prime candidates for personal medical devices and remote environmental monitoring. Furthermore, scientific developments in nanomaterials have enabled sensor modifications that greatly improve the limits of detection of existing methods due to an increased surface area and signal amplification (Hammond *et al.*, 2016).

As the demand for faster response time and more sensitive analyses increases, so does the need for electrode modifications that will fulfill these requirements while maintaining the reliability and accuracy of the existing methods. A recurring challenge is the immobilization of the biomolecule to the electrode substrate without damaging its bioactivity or selectivity to an analyte. Not only should the modification technique maximize the electron transfer between the biomolecule and the sensor transducer but it should not induce increased background noise if the electrode is to have high sensitivity and signal resolution. Ideally, the immobilization method should also be reproducible and stable over a period of time that would be realistic for practical applications. Evidently, much research has been put into optimizing the materials and modification procedures used for electrochemical biosensors in order to fulfill all of these criteria. Lately graphene and its derivatives, as well as other carbon materials with honeycomb monoatomic layer structure (e.g., carbon nanotubes, fullerenes and quantum dots), have attracted much attention for such a purpose. For example, the enzyme, ascorbic oxidase (**AO**), was immobilized during the reduction of GO and the polymerization of 3,4-ethylenedioxythiophene (**EDOT**) using cyclic voltammetry in order to form a graphene-PEDOT film that would react specifically to ascorbic acid (Lu *et al.*, 2013). It was determined that the graphene-PEDOT film had higher electroactive surface area compared to a bare electrode or one modified only with PEDOT. Consequently, the electron transfer between AO and the electrode as ascorbic acid was oxidized could be improved. The resulting biosensor demonstrated high selectivity with a limit of detection of 2 μM which confirms the preservation of AO bioactivity. It was found by another method that ascorbic acid could be detected selectively by oxidation at an electrode modified with oxidized polypyrrole (**PPyox**) and single-walled carbon nanotubes (**SWCNT**) (Li *et al.*, 2007). The PPyox layer provided a porous support for the SWCNT which resulted in greater stability of the biosensor and enhanced electron transfer while obtaining analyte detection limits down to 4.6 μM.

Such novel materials as graphene and its derivatives provide the increased surface area and electrical conductivity ideal for electrochemical biosensors, the requirement being that the graphene modification provides feasibility of the biomolecule immobilization and high affinity and selectivity for the target analyte recognition. The method used to obtain graphene derivatives is crucial when considering the material properties which will give the best sensor performance. For example, the

electrochemical reduction of GO leaves a fraction of unreduced oxygen-containing groups in the produced material compared to a chemical reduction. This results in a nitrite biosensor with lower sensitivity and selectivity compared to one based on chemically reduced GO (Mani *et al.*, 2012). It has, however, been shown that the extent of reduction, and therefore the amount of oxygen containing functional groups, can be easily controlled in the electrochemical reduction of GO by cyclic voltammetry (Guo *et al.*, 2009). This is accomplished by modifying the negative switching potential as well as the reduction time; where a more negative switching potential and a longer reduction time results in a higher degree of reduction. This provides the opportunity to determine the extent of reduction that optimizes biosensor performance. A sensor used for the detection of gallic acid in food and beverages was found to have the maximum sensitivity, selectivity and linearity when reduced at -0.90 V compared to other reduction potentials between -0.25 and -1.50 V (Hui *et al.*, 2016). This was mainly due to the extent of reduction allowing non-reduced oxygen containing functional groups that provided an affinity between the sensor and the analyte and enhanced the electron transfer. In a similar manner, the properties gained from doping of the material can be tuned to not only gain optimum electronic properties for sensor performance but to also provide the active sites required for biomolecule immobilization. The type of heteroatom used for doping, the conditions as well as the method all determine the efficiency of doping as well as the material's ability to immobilize biomolecules and detect the target analyte. The increased surface area of graphene and its derivatives not only aids in improved electron transfer but also provides the opportunity of a higher density of biomolecules immobilized on the surface. A variety of immobilization techniques exist including physical adsorption of the biomolecule based on hydrophobic interactions between the biomolecule and the graphene material. While this method is simple, the end result is biomolecules attached to the surface at random. Covalent attachment is possible when the graphene material contains functional groups that are able to covalently bind via the biomolecules' functional groups. For example, nucleic acids with an amide terminal group are covalently bound to carboxylic functional groups within the graphene material via carbodiimide/N-hydroxysuccinimide chemistry (Thermo Scientific, 2012). While this method enables direct immobilization, it is dependent on the graphene material containing enough functional groups in order to obtain sufficient coverage and density of biomolecules. Besides

the tedious and complex chemistry, direct immobilization of biomolecules at the surface of carbon materials may result in surface denaturation. This phenomenon is caused by disruption of the network of water molecules close to the surface of a material and leads to destabilization of folding of long biomolecules, especially proteins. To circumvent this problem, biomolecules can be covalently bound using a crosslinking chemistry. A crosslinker reagent contains multiple reactive chemical groups enabling it to bind to functional groups both at the graphene material surface and the biomolecule, and a spacer arm providing a distance between immobilized biomolecule and the immobilization site. With a wide variety of crosslinkers available which target functional groups such as amine, carboxyl, sulfhydryl and hydroxyl groups it is possible to choose a crosslinker reagent specific to the biomolecule to be immobilized and the functional groups present in the graphene material and preserve the native functionality of the biomolecule. The primary amines located within N-doped graphene can be used for this purpose. Amine-reactive chemical groups, such as N-hydroxysuccinimide ester and imidoester, contain carboxylic acids that react with primary amines to form amide or amidine bonds respectively. This enables the crosslinker to be attached to N-doped graphene through stable, covalent bonds at any position where a primary amine is located.

The use of crosslinking chemistry is highly effective when considering the immobilization of DNA as the biomolecule for a DNA biosensor. Double stranded DNA (**dsDNA**) consists of two single strands of DNA (**ssDNA**) with a sugar and phosphate backbone and covalently bound together up the center by complementary base-pairs; guanine only pairs with cytosine and thymine with adenine. Genetic disorders are caused by mismatches in these dsDNA base-pairs and can be identified as such. Therefore, the ability to electrochemically detect the presence of a specific sequence of DNA is highly valued as it would enable the identification of genetic disorders without the need of expensive DNA sequencing equipment and lengthy analyses. Electrochemical biosensors are strong candidates for this type of analysis as they provide the low limits of detection required for DNA analysis and can be easily adapted depending on the target DNA sequence. The biosensor is modified with a ssDNA, called the **probe**, which has the complementary sequence of the **target** DNA (**cDNA**). The biorecognition event is therefore the **formation of double helix** of the probe DNA with the target DNA in the sample forming **dsDNA**. When the double helix formation occurs at the surface of the

electrode this event is called **hybridization** and the double helix bound to the electrode surface is called a **hybrid**. With custom DNA synthesis available, it is possible to define the exact base-pair sequence as well as to add a thiol group to enable immobilization to the sensor substrate. dsDNA in itself has the affinity required for electrostatic adsorption at the electrode surface, however, this can result in the probe being attached to the surface at multiple points and hindrance of a complete cDNA hybridization. Therefore, chemical immobilization of the probe is preferred and thiol modification of one end of the probe DNA strand is crucial. For immobilization of a thiol-modified DNA probe, a crosslinking reagent requires a sulfhydryl-reactive group that would specifically react with the thiol group of the probe forming a thioether bond. Considering the purpose of the DNA probe to hybridize with target DNA in the sample, it is important to take into account the spatial configuration of the DNA probe required for successful DNA hybridization and detection. While an increased probe density would lead to greater signal amplification, it has been found that a too high density results in repulsion between the negatively charged backbones of the probe and target DNA (Peterson *et al.,* 2001). Ideally, the use of RNGO would facilitate the detection of cDNA hybridization through the immobilization of the DNA probe via crosslinking chemistry between the primary amine present at the biosensor surface and the thiol group at one end of the DNA probe. The extent of N-doping therefore has a direct impact on the density of DNA probe immobilized at the surface and thus on the success of detectable cDNA hybridization.

The current work will focus on optimizing the deposition procedure of nGO and its subsequent reduction and N-doping in order to obtain a reproducible material with maximum electroactive surface area and enhanced electron transfer. The resulting electrocatalytic properties and active sites of reduced and N-doped nanographene oxide (**RNnGO**) will be used as a platform for the immobilization of DNA probe for the electrochemical detection of ssDNA. The extent of reduction and N-doping will be determined via the detection of successful cDNA hybridization.

# 3. Experimental Section

## 3.1 Chemical reagents

Nano Graphene Oxide Solution (99% purity) was purchased from Graphene SuperMarket, USA. Lithium tetrafluoroborate, hexaammineruthenium(III) chloride, ferrocene, tris(2-carboxyethyl)phosphine hydrochloride, albumin from bovine serum, sodium chloride, sodium dihydrogen phosphate dihydrate and sodium hydroxide pellets (98% purity) were purchased from Sigma-Aldrich, Germany. Potassium nitrate, potassium hexacyanoferrate(III), trisodium citrate dihydrate (99.0% purity) was purchased from Sigma-Aldrich, Germany. Maleimidoacetic acid N-hydroxysuccinimide ester (95% purity) was purchased from Sigma-Aldrich, Germany. Acetonitrile anhydrous (99.8% purity) was purchased from Sigma-Aldrich, Germany. Deoxyribonucleic acid sodium salt from calf thymus (Type - I, fibers) was purchased from Sigma-Aldrich, USA. Sodium tetraborate decahydrate (99.5% purity) and hydrochloric acid, Titrisol® were purchased from Merck Millipore, USA. Sodium dodecyl sulfate (90%) and ethylenediaminetetraacetic acid (**EDTA**) (99.0% purity) were purchased from Honeywell Fluka, Germany. Oligonucleotides were custom ordered from Sigma-Aldrich, USA to obtain probe DNA (5'-[ThiC6]GTTGAAGGGCGGATTATATC-3, SHssODN20), complementary DNA (5'-GATATAATCCGCCCTTCAAC-3', cssODN20), and non-complementary DNA target (**ncDNA)** (5'-TGC AGC GCA ATT CAG GCG CA-3', ncssODN20).

## 3.2 Apparatus

All characterizations by cyclic voltammetry and electrochemical impedance spectroscopy were done using an IviumStat.h from Ivium Technologies (The Netherlands). Scanning electron microscope (**SEM**) measurements were carried out by Linus Silvander at the Laboratory of Inorganic Chemistry, Åbo Akademi University (LEO Gemini 1530, Oberkochen, Germany).

## 3.3 Preparation of solutions

50 mM phosphate buffered saline (**PBS**) with ionic strength of 0.5 M (NaCl), was prepared from sodium dihydrogen phosphate dihydrate and sodium chloride dissolved in deionized water. The pH was adjusted to 7.00 with 1 M NaOH and diluted to a total volume of 1 L.

100 mM borate buffer was prepared by weighing 0.76 g of disodium tetraborate decahydrate dissolved in 12.5 mL of deionized water. 1.15 mL of 0.1 M HCl was added to this borate solution and then diluted to 25 mL with deionized water.

The supporting electrolyte for the reduction and N-doping of graphene oxide was prepared by measuring approximately 0.5 g of lithium tetrafluoroborate and drying it at 60°C for 1 hour under reduced pressure. A 0.1 M solution was made from measuring 0.468 g of the dried chemical and dissolving it in acetonitrile (**ACN**).

The redox properties of various redox couples were used throughout the experiments. 1 mM hexaammineruthenium(III) chloride was prepared by dissolving 30.98 mg in PBS. 1 mM ferrocene was prepared by dissolving 1.86 mg in 0.1 M $LiBF_4$ in ACN. 1 mM hexacyanoferrate was prepared by dissolving 16.47 mg in 1 M $KNO_3$.

1 mM maleimidoacetic acid N-hydroxy succinimide ester was prepared by dissolving 0.77 mg in borate buffer with the aid of an ultrasonic bath.

A stock solution of saline sodium citrate buffer (**20X SSC**) was prepared by with 300 mM trisodium citrate and 3 M sodium chloride made from dissolving 4.41 g and 8.77 g, respectively, in deionized water. The solution was titrated with 1 M HCl to give a pH of 7.00. The stock solution was consequently diluted with deionized water to give 2X, 1X and 0.5X solutions to be used for washing of the electrodes after probe immobilization.

0.1 % w/v sodium dodecyl sulfate (**SDS**) was prepared by weighing 25.0 mg and dissolving it in 25 mL of deionized water.

Bovine serum albumin (**BSA**) was used as a blocking solution to cover bare spots on the electrode surface and avoid non-specific absorption of DNA in the sample. A 2 % w/v solution was prepared by dissolving 80 mg in 4 mL of deionized water.

A 10X calf thymus DNA (**CT-DNA)** solution was prepared with deionized water and $10^{-4}$ M EDTA. To aid with the dissolution and breaking of the DNA strands, the solution was passed through a syringe approximately 40 times or until the solution was visibly less viscous. The solution was placed in an ultrasonic bath for 10 min for further chain fragmentation. In the final step the fragmented DNA chains were denatured by keeping the solution for 10 min in boiling water followed by immediate chilling in an ice bath for 10 min. This stock solution was then used to prepare a blocking solution as an alternative to BSA. 47.0 µL of calf thymus DNA stock solution was combined with 94.0 µL of $10^{-4}$ M EDTA, 1412.0 µL 20X SSC and 2447.0 µL of deionized water for a total volume of 4 mL.

## 3.4 Preparation of Ag/AgCl reference electrode

A silver wire was chlorided in 1 M NaCl with an applied current of 0.1 mA for 4 hours using a coulometer (Type E211, Metrohm AG, Herisau, Switzerland). The standard potential was measured against 1 mM ferrocene in 0.1 M $LiBF_4$ in ACN by cyclic voltammetry with a potential range from 0.0 to 0.7 V for 5 cycles with scan rate of 0.05 V/s. The mean value of the cathodic and anodic peak potentials from each of the five recorded CVs was taken to be the standard potential.

## 3.5 Preparation of electrodes

Working disk electrodes for microscopic characterization were manufactured in house by inserting a glassy carbon rod (⌀ = 3 mm, $l$ = 2 cm, Alfa Aesar) into a cylindrical Teflon casing. The surface of the glassy carbon was polished using sand paper (grits from 320 to 4000) followed by diamond paste (15 to 1 µm) and 0.3 µm $Al_2O_3$ on polishing pads to obtain a mirror finish. They were then sequentially cleaned in 1M $HNO_3$, ethanol and deionized water in an ultrasonic bath. Finally they were placed in an Argon plasma cleaner for 10 minutes to remove any remaining contaminants and to obtain a more hydrophilic surface.

Glassy carbon disk electrodes for electrochemical analysis were purchased from BASi (MF-2012). The diameter of disk is 3.0 mm. The electrodes were only polished with diamond paste and $Al_2O_3$ on polishing pads as they came already pre-polished to a mirror finish.

## 3.6 Surface area characterization

The active surface area of each of the bare electrodes was calculated by applying the Randles-Sevcik equation. In a cell containing 1 mM $K_3[Fe(CN)_6]$ in 1.0 M $KNO_3$ and purged with $N_2$, cyclic voltammograms were recorded with a potential range from -0.2 to 0.75 V. The potential step was 10 mV and the scan rate was varied from 0.005 to 0.2 V/s.

The bare electrodes were also characterized in 1 mM ferrocene in 0.1 M $LiBF_4$ in ACN by cyclic voltammetry with an applied potential range from -0.15 to 0.7 V for 5 cycles. The potential step was 10 mV and the scan rate was 0.05 V/s. The impedance was measured by electrochemical impedance spectroscopy (**EIS**) in 50 mM PBS at open circuit potential (**OCP**) with frequencies from 10 kHz to 10 mHz.

## 3.7 Optimization of drop casting

Nanographene oxide (**nGO**) ( 1 g/L solution in water, Graphene SuperMarket) was cast onto the glassy carbon surface in 5 μL aliquots (approximately 5 μg of nGO per aliquot) with drying in between. The electrodes were then annealed under reduced pressure at 60°C for varying durations. To examine the surface coverage the modified electrodes were analysed using cyclic voltammetry: 5 cycles were recorded within the range of potentials -0.15 to 0.7 V in 1 mM ferrocene solution in ACN with 0.1 M $LiBF_4$ as supporting electrolyte at a scan rate of 0.05 V/s. The number of drop castings were repeated until there was no significant decrease of the faradaic peak currents. After that two additional 5 μL aliquots of nGO were cast to the electrode surface to make sure that the electrode surface remained completely covered with the material after its shrinkage due to the electrochemical reduction of nGO.

## 3.8 Reduction and N-doping of graphene oxide

nGO cast on the electrode surface was reduced and doped with nitrogen in a solution of 0.1 M $LiBF_4$ in ACN. In the conventional three-electrode setup, a glassy carbon (**GC**) rod was used as the counter electrode and an Ag/AgCl wire as the reference electrode. The solution was purged for 10 min with $N_2$ prior to reduction and a nitrogen atmosphere was sustained throughout the reduction process. The reduction was carried out by staircase waveform cyclic voltammetry by performing 30 scans within the potential range of -2.6 to +0.385 V against $Fc/Fc^+$ standard potential with a potential step of 10 mV and a scan rate of 0.05 V/s.

To compare reduction and N-doping with solely reduction, nGO was reduced in 0.1M $LiBF_4$ in propylene carbonate under the same conditions and parameters.

## 3.9 Electrode characterization

Obtained reduced and N-doped nanographene oxide (**RNnGO**) modified GC electrodes (**GCE**) were characterized by cyclic voltammetry and electrochemical impedance spectroscopy with a variety of solutions and parameters: 1 mM $[Ru(NH_3)_6]Cl_3$ in PBS with a potential window of -0.6 to 0.2 V and a scan rate of 0.5 V/s, 1 mM ferrocene in 0.1 M $LiBF_4$ in ACN with a potential window of -0.15 to 0.7 V and a scan rate of 0.05 V/s, and 1 mM hexacyanoferrate in 1 M $KNO_3$ with a potential window of -0.15 to 0.7 V and a scan rate of 0.05 V/s. The number of scans recorded was 5. The stability of RNnGO in aqueous media was tested by cyclic voltammetry in 50 mM PBS (I=0.5 M, pH 7.0) from -0.6 to 0.2 V with a scan rate of 0.1 V/s for 100 cycles. The electrochemical

properties of RNnGO and reduced nGO (**RnGO**) were compared through characterization by cyclic voltammetry in 1 mM hexacyanoferrate in 1 M $KNO_3$ with a potential window of -0.15 to 0.7 V at scan rates varying from 0.01 to 0.2 V/s. The cell electrolyte was first purged for 10 min with $N_2$ and a nitrogen atmosphere was sustained throughout the measurements. All electrochemical measurements were done with a conventional three-electrode system with a glassy carbon counter electrode, 3 M KCl Ag/AgCl reference electrode in aqueous solutions and an Ag/AgCl wire in organic solutions. Prior to recording CVs in the solutions containing redox couples the CVs of background electrolytes were recorded.

EIS measurements were done in 50 mM PBS (I=0.5 M, pH 7.0) with a frequency range of 0.1 Hz to 100 kHz at the open circuit potential and with an amplitude of 5 mV.

## 3.10 Fabrication of a biosensor: Tethering of DNA probe to the reduced N-doped nanographene oxide surface and blocking its free sites

In order to activate nitrogen-bearing sites at the surface of RNnGO (primary amino groups) for attachment of thiolated DNA probe, GC electrodes modified with NRnGO were incubated in the crosslinking solution (maleimidoacetic acid N-hydroxysuccinimide ester) for 1.5 hours at room temperature. Then the electrodes were rinsed with PBS and incubated for 2 hours in a 37°C water bath containing 0.5 μM DNA probe and 10 mM tris(2-carboxyethyl)phosphine hydrochloride in PBS. Afterwards, each electrode was washed 3 x 1 mL with 0.1 w/v% SDS, SSC 2X, 1X, 0.5X and deionized water subsequently in order to remove DNA strands non-specifically adsorbed to RNnGO surface. The free sites of RNnGO unoccupied with DNA strands were blocked either by incubation in BSA or in CT-DNA for 1 hour at room temperature. The electrodes were washed 3 x 1 mL with PBS and deionized water and stored at 4°C.

The extent of DNA probe cross-linking was measured by incubating the electrodes in 1 mM $[Ru(NH_3)_6]Cl_3$ in PBS for 5, 30 and 60 minutes followed by recording CVs in nitrogen purged 1 mM $[Ru(NH_3)_6]Cl_3$ in PBS. 5 scans were performed with a potential range of -0.6 to 0.2 V and a scan rate of 0.5 V/s. A 3 M KCl Ag/AgCl electrode was used as reference electrode and a glassy carbon rod as counter electrode. After measuring, the electrodes were washed 3 x 1 mL with PBS and incubated in PBS for 30 min.

## 3.11 Response of the biosensor to the hybridization of the DNA probe with non-complementary and complementary DNA target

The electrodes modified with RNnGO and DNA probe were first tested for sensitivity to non-complementary DNA (**ncDNA**) due to non-specific adsorption of DNA strands to the surface of the electrode material. To do that, the electrodes were incubated in a 0.5 μM solution of ncDNA and PBS for 1 hour in a 37°C water bath. They were then washed 1 x 1 mL with PBS and incubated in 1 mM $[Ru(NH_3)_6]Cl_3$ in PBS for 5 min. Afterwards, the electrodes were characterized by CV; the voltammograms were recorded in a nitrogen purged cell containing 1 mM $[Ru(NH_3)_6]Cl_3$ in PBS. 5 scans were performed with a potential range of -0.6 to 0.2 V *vs* Ag/AgCl (Metrohm, 3 M KCl) and a scan rate of 0.5 V/s using a GC rod as counter electrode. Immediately after measuring, electrodes were washed 3 x 1 mL with PBS and incubated in PBS for 30 minutes.

To further test the biosensors for selectivity to a complementary sequence of DNA (selective adsorption to the surface of the electrodes), the electrodes were incubated in a 0.5 μM solution of complementary DNA (**cDNA**) in PBS for 30 minutes in a 37°C water bath. After each allotted amount of time, the electrodes were washed with 1 mL of PBS and incubated in 1 mM $[Ru(NH_3)_6]Cl_3$ in PBS for 5 min. CVs were recorded in a nitrogen purged cell containing 1 mM $[Ru(NH_3)_6]Cl_3$ in PBS. 5 scans were performed with a potential range of -0.6 to 0.2 V and a scan rate of 0.5 V/s. Immediately after measuring, the electrodes were washed 3 x 1 mL with PBS and replaced in the cDNA solution. These steps were repeated for incubation for another 30 min and 2 hrs in a 37°C water bath (1 hour and 3 hours total) in order to monitor the kinetics of hybridization of the probe and the complementary target. After the final washing with PBS, the electrodes were incubated in PBS for 30 min before air drying and storing at 4°C.

# 4. Results and Discussion

## 4.1 Determination of Electrochemical Surface Area

In electrochemical sensors the reproducibility of their performance is determined by numerous factors, among them the surface area of an electrode involved in an electrochemical reaction is one of the most important. While it is straightforward just to measure the geometric surface area of an electrode, it is not sufficient because the materials used for electrode preparation may contain different amounts of the reactive sites due to *e.g.* different surface roughness, chemical structure, and presence of defects. Therefore in order to standardize the electrochemically active area must be determined through alternate methods, for example, by using Randles-Sevcik equation (Equation 1).

$$I_p = 0.4463nFAC\left(\frac{nF\upsilon D}{RT}\right)^{\frac{1}{2}} \quad (1)$$

$I_p$ is peak current, $n$ is the number of redox electrons, $F$ is Faraday's constant, $A$ is the electrode area, $C$ the concentration of the redox couple in the solution, $\upsilon$ is the scan rate, $D$ is the diffusion coefficient of the redox couple, $R$ *is* the gas constant and $T$ is the temperature. The diffusion coefficient of $K_3[Fe(CN)_6]$ redox couple is known to be 7.6 x $10^{-6}$ $cm^2/s$ (Stackelberg *et al.* 1953).

To determine the electrochemical surface area of the GC electrodes, we recorded CVs of the solutions of the redox couple at different scan rates. The maximum values of the anodic and cathodic peak currents of oxidation and reduction of $Fe^{2+}/Fe^{3+}$ ions were then plotted versus the square root of the scan rate to find the slope of the resulting linear plots (Figure 1).

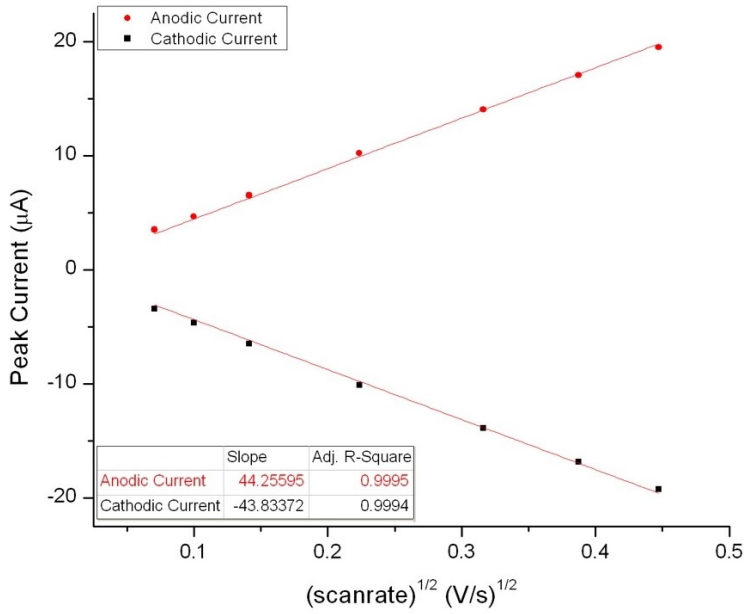


*Figure 1: Dependence of peak current on scan rate according to the Randles-Sevcik equation. Anodic and cathodic peak currents attained through cyclic voltammetry in 1 mM $K_3[Fe(CN)_6]$ in 1.0 M $KNO_3$ from +0.2 to +0.75 V vs Ag/AgCl/3 M KCl with varying scan rates of 0.005, 0.01, 0.02, 0.05, 0.1, 0.15, 0.2 V/s.*

By rearranging equation 1, it is possible to relate the slope to the electrochemical surface area of the electrode (equation 2).

$$A = \frac{slope}{(2.69\times10^5)n^{\frac{3}{2}}D^{\frac{1}{2}}C} \quad (2)$$

Each slope from the anodic and cathodic peak currents was used to calculate corresponding surface areas for each electrode. For commercial glassy carbon electrodes, the average electrochemical surface area was (0.056±0.002) $cm^2$ while for hand polished electrodes the average was (0.059±0.004) $cm^2$. The electrochemical surface area determined in this manner was used for further calculations.

## 4.2 Modification of glassy carbon electrodes with graphene oxide.

### 4.2.1 Optimization of drop-casting protocol: number of 5-µL aliquots

Due to the latest popularity of graphene and its derivatives in electrochemistry there is a large number of publications about modification of electrodes with graphene oxide and reduced graphene oxide. Typically the researchers utilize an electrochemical co-deposition of GO with, for example, conducting polymers. Another group of authors report modification of the electrodes by drop casting GO onto their surface however it is highly doubtful that the way of drop casting of this material can be done in a very reproducible manner, mainly due to the fact that single drop casting of a small amount of GO solution does not lead to complete surface coverage leaving voids and causing false positive response in analytical applications. Cyclic voltammetry or any other electrochemical method involving measurements of electrochemical activity of the electrode material upon the process of deposition of GO can conveniently be used to monitor the efficiency of the electrode coverage. In our work we chose CV as the most commonly used electrochemical method for materials characterization in our laboratory, and $K_3[Fe(CN)_6]$ was used as an electrochemically active salt.

Due to nGO being non-conducting, the decrease in peak current upon nGO deposition is related to the reduction of electrochemically active surface area of the electrodes as a result of their surface coverage with the sheets of nGO. One could therefore presume that the complete coverage of the surface would result in complete blocking of the access of electrochemically active species to the surface of the electrode and the resulting CV shall be similar to the CV of the background electrolyte where no $K_3[Fe(CN)_6]$ is added (Figure 2).

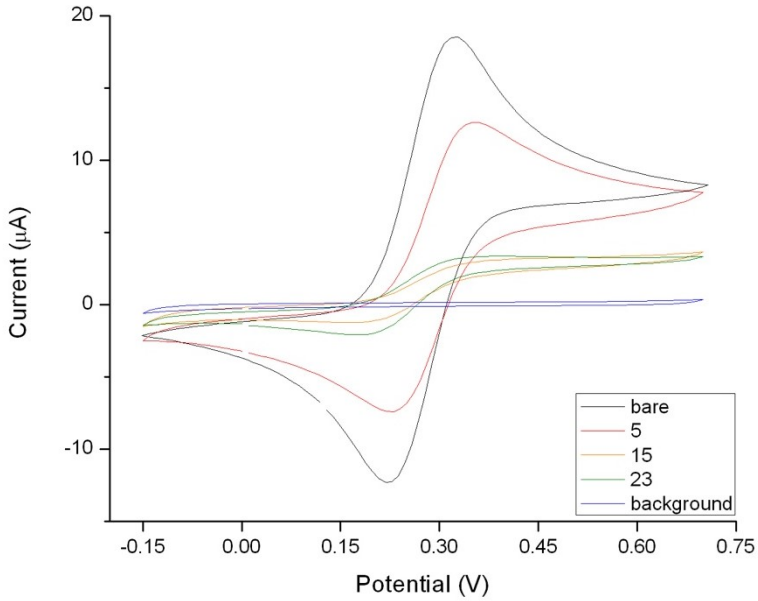


*Figure 2: Optimization of electrode surface coverage by drop-casting increasing 5-μL aliquots of 1 g/L nGO. Cyclic voltammetry in 1 mM ferrocene in 0.1 M $LiBF_4$ in ACN from -0.15 to 0.7 V vs Ag/AgCl wire with a scan rate of 0.05 V/s.*

After each 5-μL aliquot is cast, it is left to air dry in ambient conditions devoid of significant air flow to ensure a uniform drying. In Figure 2 it is seen that after addition of 5 aliquots of nGO solution (25 μL collectively) the peak currents of $Fe^{3+}/Fe^{2+}$ have diminished by ca. 35% indicating partial coverage of the surface of GC with nGO. Additions of 15 aliquots of nGO (75 μL collectively) reduced the peak current down to 86% of the initial current of bare electrode. This, however, seemed to be the limit since further additions of up to 23 aliquots of nGO (115 μL collectively) did not improve the reduction of peak currents close to the level of the background currents. It is known from the literature that graphene oxide forms channels in the areas of stacking graphene sheets next to each other and in interplanar spacing due to entrapment of water between sheets upon casting (Devanathan *et al.,* 2016). Therefore such channels can serve as pathways for ions of iron redox couple to migrate towards the electrode surface and to be electrochemically reduced and oxidized. Therefore we speculated that the removal of entrapped water can, at least partially, improve the surface coverage of GC with nGO sheets and reduce current of the CVs of the redox couples as a consequence.

### 4.2.2 Optimization of drop-casting protocol: thermal annealing

Annealing is often employed to alter the physical and chemical properties, such as bonding and electrical conductivity, of a semiconductor or metal interface (Yamaguchi *et al*., 2014). In the case of the GC and nGO interface, annealing would remove remaining water entrapped between the nGO layers and possibly improve the electrode surface coverage. Annealing of the electrodes was carried out under reduced pressure at 60°C. As shown in Figure 3, the annealing of the electrodes

modified with 5 5-µL aliquots of nGO did not decrease the peak currents. In fact, the peak currents increased by 2% despite annealing. However, annealing of the electrodes modified with 23 5-µL aliquots of nGO showed a 42% decrease in peak currents and almost no apparent redox peaks. This is due to the incomplete surface coverage of the bare GC electrode with only 5 5-µL aliquots of nGO which allows for access of the redox couple to the surface despite annealing. Applying 23 5-µL aliquots, however, provides a more complete surface coverage which can then be improved by removing the remaining water and sealing of the nGO material to block the majority of the redox couple gaining access to the surface of glassy carbon electrode.

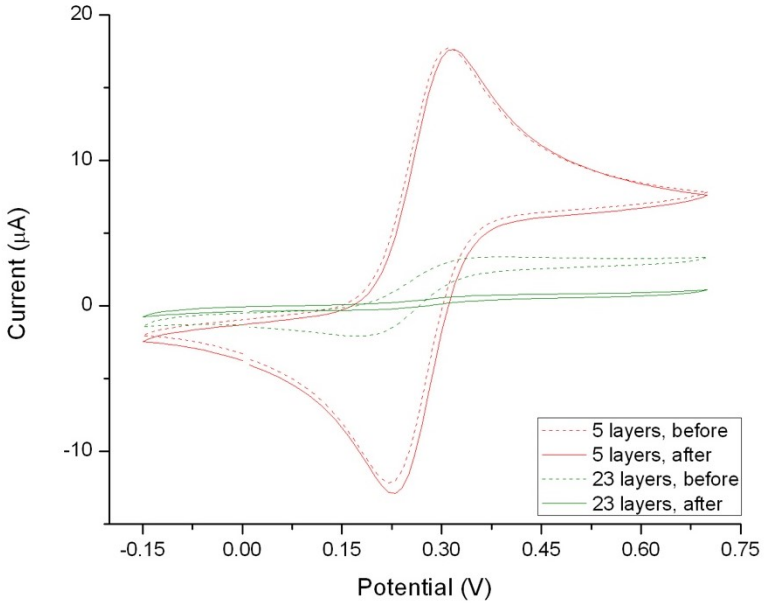


*Figure 3: CVs recorded before and after annealing to determination its effect on total electrode surface coverage with 5 and 23 5-µL aliquots of nGO. Cyclic voltammetry in 1 mM ferrocene in 0.1 M $LiBF_4$ in ACN from -0.15 to 0.7 V vs Ag/AgCl wire with a scan rate of 0.05 V/s.*

The optimum annealing duration was determined by annealing electrodes cast with 23 5-µL aliquots of nGO for 30 minutes, 1 hour, and 8 hours and recording their CVs in the ferrocene solution afterwards, as shown in Figure 4.

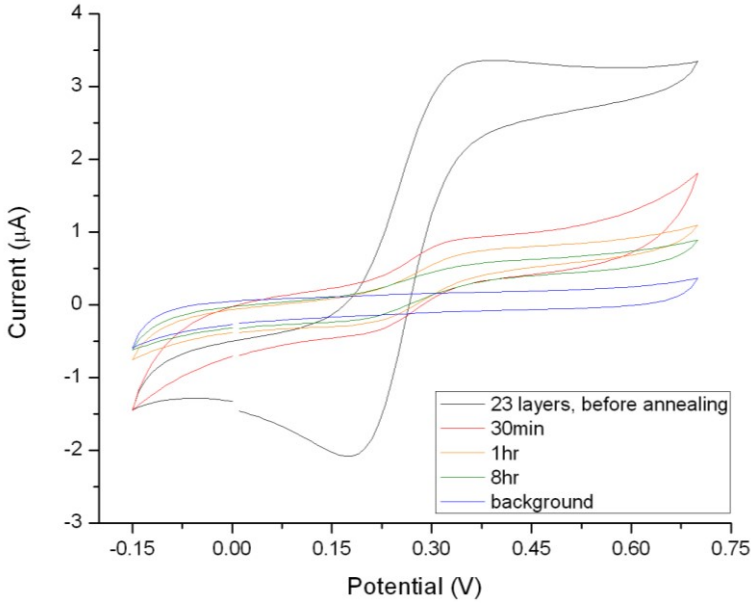


*Figure 4: Optimization the duration of annealing electrodes under vacuum at 60°C. Cyclic voltammetry in 1 mM ferrocene in 0.1 M $LiBF_4$ in ACN from -0.15 to 0.7 V vs Ag/AgCl wire with a scan rate of 0.05 V/s.*

There was a 75% decrease of the redox current after annealing of the electrodes modified with 23 5-µL aliquots of nGO for 30 minutes and a 81% decrease after 1 hour. However, further thermal treatment of the electrodes for 8 hours only showed an 85% decrease of redox current compared to before annealing. It was therefore determined that drop-casting 15 5-µL aliquots of nGO, for a total drop-cast amount of 75 µg of nGO, and annealing for 1 hour was enough to attain sufficient coverage of the electrode surface. 2 additional aliquots were added to account for the shrinkage of nGO upon reduction.

### 4.2.3 SEM characterization: Not annealed surface *vs* annealed surface, pinholes, bright spots, homogeneity.

The effect of annealing on the surface characteristics of the modified electrodes was characterized by Scanning Electron Microscopy (**SEM**) (Figure 5).

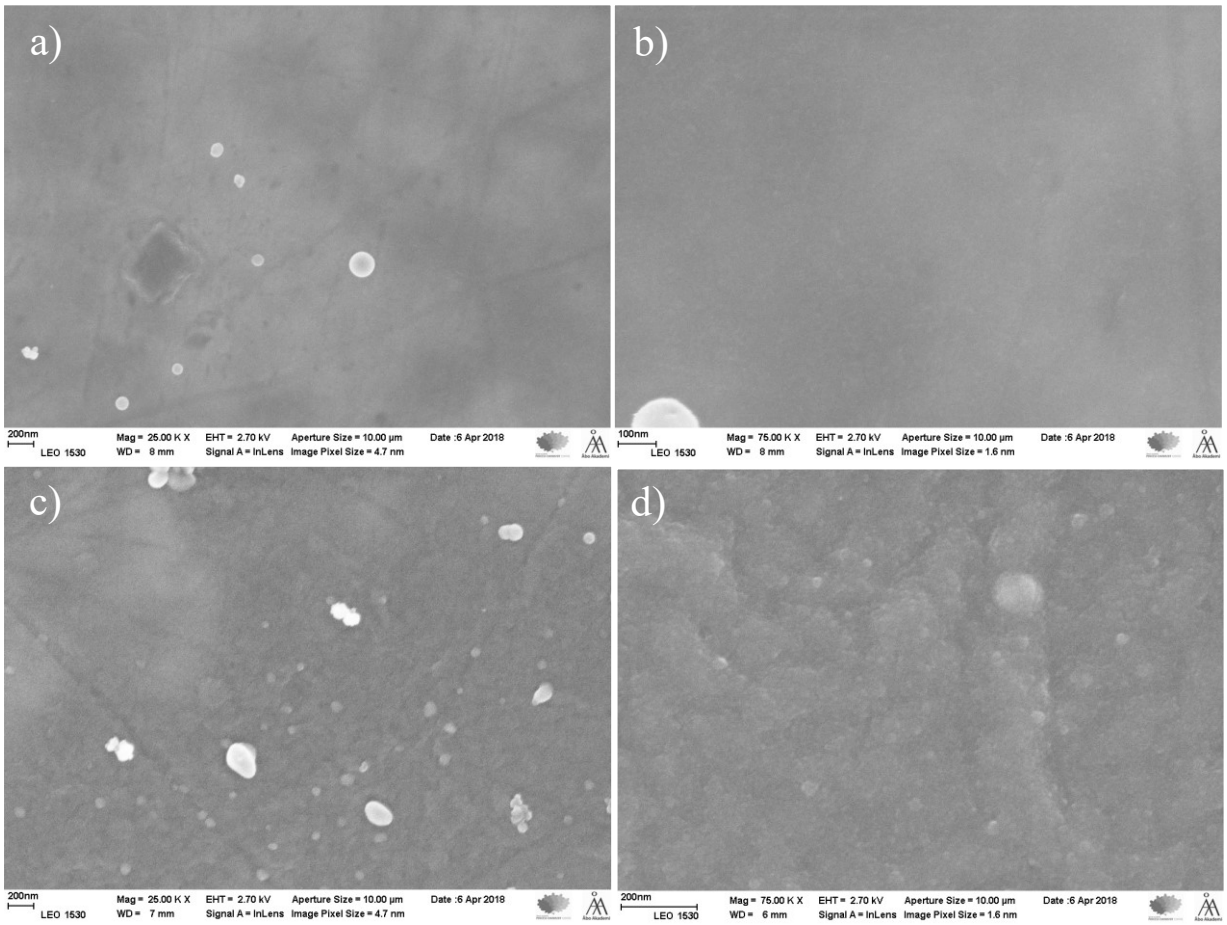


*Figure 5: SEM characterization of electrode with 15 layers of nGO before annealing (a, b) and after annealing for 1 hour at 60°C (c, d). SEM images are shown from two different spots on the electrode and with 25 kx and 75 kx magnification.*

nGO has been characterized as small flakes suspended in aqueous solution (Marcano *et al.*, 2010). Once drop-cast onto the surface, it is allowed to dry under ambient conditions which allows an even distribution of GO across the surface. Images of the nGO surface without annealing are homogeneous, showing very little contrast in brightness (Figure 5 a., b.). The surface is smooth and featureless apart from a small number of dark patches that could be explained by the inconsistency of air drying resulting in varying thicknesses of nGO after drop-casting. Upon annealing, the remaining aqueous solution evaporates from between the flakes, causing them to become shriveled and uneven. SEM images of the electrode surface with annealing show these prominent contrasts in morphology (Figure 5 c., d.). The surface appears rough and contains more topographical features which can be explained by the extent of evaporation of any remaining water within the nGO surface.

### 4.2.4 Dissolution of nGO

nGO is not electrochemically conducting and therefore does not partake in electron transfer of redox reactions. Therefore increase of current of redox reaction (for example, $Fe^{2+}/Fe^{3+}$) after reduction of nGO is indicative for restoration of polyconjugated structures of graphene sheets. However it might happen that nGO is partially soluble in ACN and therefore the increase of electrochemical activity after reduction is attributed to partial removal of nGO from the electrode surface. In order to show that dissolution does not play a significant role in the increase of the electrochemical activity of the GCE modified with nGO we carried out a test for the dissolution of nGO in an organic solvent by performing cyclic voltammetry of GCE with drop-cast and annealed nGO in the presence of a redox couple. Figure 6 shows CVs from the 2nd cycle to the 50th along with their determined charge capacities (derived through integration of CV). There is, in fact, a 12.9 µC reduction, 7.6% of the total charge capacity, which shows that nGO is not soluble in organic solution and therefore its dissolution does not contribute to the increase of electrochemical activity of the electrodes modified with nGO upon its reduction.

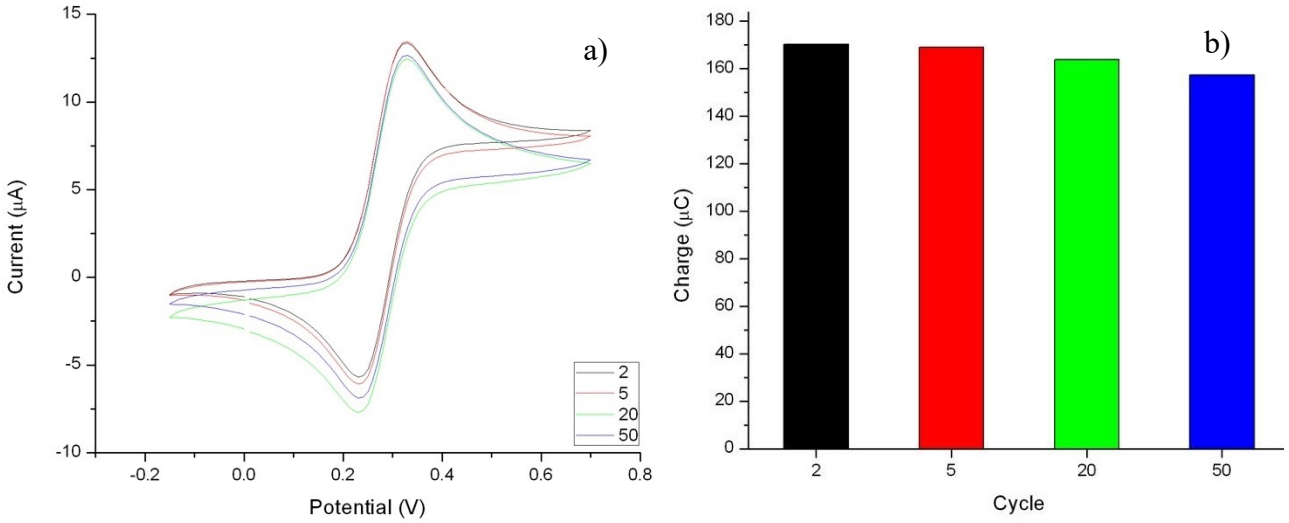


*Figure 6: a) Test of dissolution of nGO in organic solution. Electrode with 5 5-µL drops of nGO cast onto the surface in a solution of 1 mM ferrocene in 0.1 M LiBF4 in ACN. CVs of 50 cycles were run from -0.15 to 0.7 V vs Ag/AgCl wire at a scan rate of 0.05 V/s. Shown are cycles 1, 5, 20 and 50. b) Change in measured charge capacity of electrode surface over 50 cycles.*

## 4.3 Reduction and N-doping of nGO drop cast on GCE

### 4.3.1 Determination of window of potentials for reduction and N-doping of nGO

The first experiments on determination of the window of potentials for reduction of nGO were carried out jointly by Eszter Supala and I, initially they were a part of another project and then continued as a part of my master's thesis work. The variation of the width of the window of reduction potential was studied in relation to whether the electrodes showed selectivity for cDNA vs ncDNA. The span of the reduction potential window, and therefore the extent of reduction and N-doping of nGO, affects the subsequent modifications of the electrode significantly. The amine groups introduced into the graphene structure react with the ester groups of the crosslinker while the crosslinker's maleimide group reacts with the thiol groups of the DNA probe. A greater extent of N-doping would result in a greater density of DNA probe on the electrode surface, however, this does not translate directly to successful selectivity of the electrodes toward DNA target. Selectivity towards cDNA is defined as the largest surface density of probe DNA capable to bind target DNA after incubation in cDNA as compared to ncDNA and give detectable electrochemical response. In the case that the electrode has a very small amount of binding sites available for immobilization of DNA probe, the sensing of a complementary strand of DNA is inefficient because it would statistically require too much time for two DNA strands to hybridize and produce an electrochemical response. Consequently, the response would be difficult to detect. On the contrary, if the amount of the DNA probe immobilized at the surface of the electrode is too large, the hybridization would be less efficient due to high density of the probe and hence steric hindrances and electrostatic repulsion. We therefore expected that the response of the biosensor would have a bell shape function of the window of potentials. The largest electrochemical response would then be observed for the material having the optimal amount of amino groups at its surface available for the immobilization of DNA probe.

DNA surface density can be determined through a quantitation method specific to DNA biosensors and their surface characterization by cyclic voltammetry. Due to the negatively charged backbones of DNA strands, sodium ions, $Na^+$, from the DNA backbone are exchanged for cations present in the solution. In the case of these experiments, they are $[Ru(NH_3)_6]^{3+}$ ions from the electrolyte solution that are partitioned into the DNA strands. As $[Ru(NH_3)_6]^{3+}$ is the oxidized form of the redox couple $[Ru(NH_3)_6]^{3+/2+}$, it is possible to see redox peaks when cyclic voltammetry is performed within a potential window of -0.6 to 0.2 V *vs* Ag/AgCl/3 M KCl. The anodic peak (negative to positive potential sweep) is the oxidation of $[Ru(NH_3)_6]^{2+}$ to $[Ru(NH_3)_6]^{3+}$ and the

cathodic peak (positive to negative potential sweep) is the reduction of $[Ru(NH_3)_6]^{3+}$ to $[Ru(NH_3)_6]^{2+}$. This electron transfer is measured as faradaic current in cyclic voltammetry. The total charge transported by the amount of current in a given amount of time, in coulombs, can be extracted from the cyclic voltammogram data either by integrating the resulting CV or by recording the charge simultaneously with the CV measurements. In our case, the data is initially recorded as measured current as a function of applied potential which can be converted to measured current as a function of time according to the scan rate used in V/s. The charge due to the faradaic current of the redox couple only can be determined by integration of the curve and subtraction of the equivalent CV performed exclusively in the electrolyte solution which accounts for the non-faradaic current. For DNA-modified biosensors, the measured charge due to electron transfer can be related to the total amount of $[Ru(NH_3)_6]^{3+}$ present within the DNA strands at the electrode surface (Equation 3), where $Q$ is the charge, $n$ is the number of electrons in the redox reaction, $A$ is the area of the working electrode and $\Gamma_{Ru}$ is the total amount of $[Ru(NH_3)_6]^{3+}$ at the electrode surface in molecules/cm$^2$ (Yu *et al*,. 2003).

$$Q = nFA\Gamma_{Ru} \tag{3}$$

The surface concentration of $[Ru(NH_3)_6]^{3+}$ can be directly related to the surface density of DNA according to Equation 4, where $z$ is the charge of the redox molecule, $m$ is the number of nucleotide bases in the DNA probe, and $N_A$ is Avogadro's number.

$$\Gamma_{DNA} = \Gamma_{Ru}(\frac{z}{m})N_A \tag{4}$$

This method was used to determine the extent of reduction and N-doping that would result in most successful hybridization of cDNA with the DNA probe. CVs were measured after DNA probe immobilization and incubation in 1 mM $[Ru(NH_3)_6]Cl_3$ in PBS for 1 hour in order to determine the DNA probe density. Successful hybridization was assessed by incubating the sensor modified with DNA probe in solutions containing ncDNA or cDNA followed by incubation in 1 mM $[Ru(NH_3)_6]Cl_3$ in PBS and characterization by cyclic voltammetry (Figure 7).

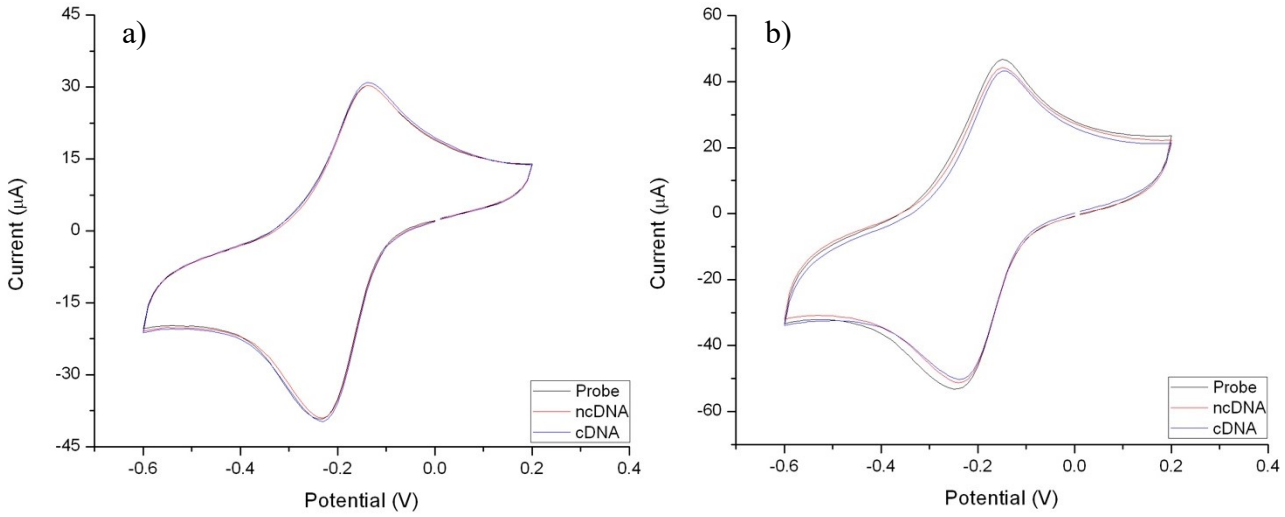


*Figure 7: DNA biosensor exhibiting selectivity (a) and non-selectivity (b) towards complementary DNA. Characterization of electrode surface by cyclic voltammetry in 1 mM $[Ru(NH_3)_6]Cl_3$ in 50 mM PBS (I=0.5 M, pH 7.0) from -0.6 to 0.2 V with a scan rate of 0.5 V/s. After probe immobilization and incubated in 1 mM $[Ru(NH_3)_6]Cl_3$ for 1 hour, after incubation in ncDNA for 1 hour and after incubation in cDNA for 30 minutes.*

Table 1 compares the different reduction potential windows and their effect on the RNnGO electrochemical properties and performance of the DNA biosensor. Drop-cast nGO was first reduced and N-doped by cyclic voltammetry with the defined potential window. The resulting RNnGO modified electrode was characterized by cyclic voltammetry in the presence of a redox probe and the surface charge was calculated as explained previously. After immobilization of the DNA probe, the sensor was incubated in $[Ru(NH_3)_6]Cl_3$ for 1 hour to allow for intercalation of the cations to the probe DNA backbone before performing CVs to determine the surface density of the DNA probe. Finally, the DNA biosensor was tested for selectivity for cDNA by incubation in solutions containing ncDNA or cDNA followed by $[Ru(NH_3)_6]Cl_3$ and characterization by CV. A sensor is considered to have positive selectivity when the calculated DNA surface density is greater after incubation in cDNA as compared to ncDNA and the difference between them is defined as the signal amplitude.

*Table 1: Modified electrode surface characterizations for different reduction potential windows.*

| **Potential Window (V)** | **Average Charge of RNnGO characterization (μC)** | **DNA Probe density (mol/cm$^2$)** | **Percent positive selectivity (%)** | **Signal amplitude for cDNA vs ncDNA (mol/cm$^2$)** |
|---|---|---|---|---|
| *-1.445 to +0.385* | 48 ± 6 | (5 ± 1)E+14 | ***0 %*** | **--** |
| *-1.830 to +0.385* | 32 ± 6 | (5 ± 1)E+14 | ***80 %*** | (1 ± 1)E+13 |
| *-2.215 to +0.385* | 33 ± 7 | (5 ± 2)E+14 | ***73 %*** | (4 ± 3)E+13 |
| *-2.6 to 0.385* | 38 ± 5 | (5 ± 1)E+14 | ***58 %*** | (2 ± 2)E+13 |

The narrowest potential window, -1.445 to +0.385 V, showed high charge during characterization after reduction and N-doping as well as a high calculated DNA probe density. However, none of the electrodes were selective towards cDNA. This is most likely due to incomplete

reduction of nGO which is soluble in aqueous solutions. Since all subsequent characterizations were done in an aqueous electrolyte solution, leftover nGO on the electrode surface would have dissolved leaving bare spots and a possibility for direct electron transfer between the bare electrode and the redox couple, therefore increasing the measured charge values. The widest potential window, -2.6 to +0.385 V, showed relatively high probe density due to it containing the highest amount of N-doping. However, only 58% of the sensors tested showed selectivity towards cDNA. This could be due to overcrowding of the electrode surface during probe immobilization and a limitation on the amount of cDNA able to hybridize with the probe due to electrostatic and steric hindrances. The reduction potential windows of -1.820 to +0.285 V showed the highest percent of positive selectivity for cDNA. However, when comparing the difference in signal amplitude, the potential window of -2.215 to +0.385 V resulted in the greatest difference in DNA surface density between ncDNA and cDNA. This could be related to the extent of N-doped being greater for the wider potential window while still allowing sufficient space for cDNA to hybridize with the DNA probe immobilized on the surface. While the narrower potential range may allow for a slightly higher success rate of cDNA hybridization, the lower DNA probe surface density does not allow for a high signal resolution between ncDNA and cDNA. The potential window of -2.215 to +0.385 V was therefore chosen as the optimum reduction potential window for the following experiments.

### 4.3.2 Reproducibility of Reduction and N-doping of nGO

In the previous experiment on optimization of the window of potentials for the reduction and N-doping of nGO we used only 5 5-µL aliquots for modification of GCE. The results of the study has shown that 5 5-µL aliquots do not cover the entire working electrode since redox peaks are visible when the electrodes modified with nGO are analyzed with CV in ACN. While nGO is nonconducting, if bare glassy carbon is exposed to the electrolyte solution containing a redox couple, reduction and oxidation is made possible through direct electron transfer between GC and the electrolyte solution. drop-casting 17 5-µL aliquots of nGO followed by annealing for 1 hour at 60°C, however, has shown to provide a much more complete surface coverage of the working electrode. The effect of surface coverage and the resulting electrode-to-electrode reproducibility of the subsequent reduction and N-doping of nGO is demonstrated in the cyclic voltammograms in Figure 8 and in the calculated surface charge values in Table 2.

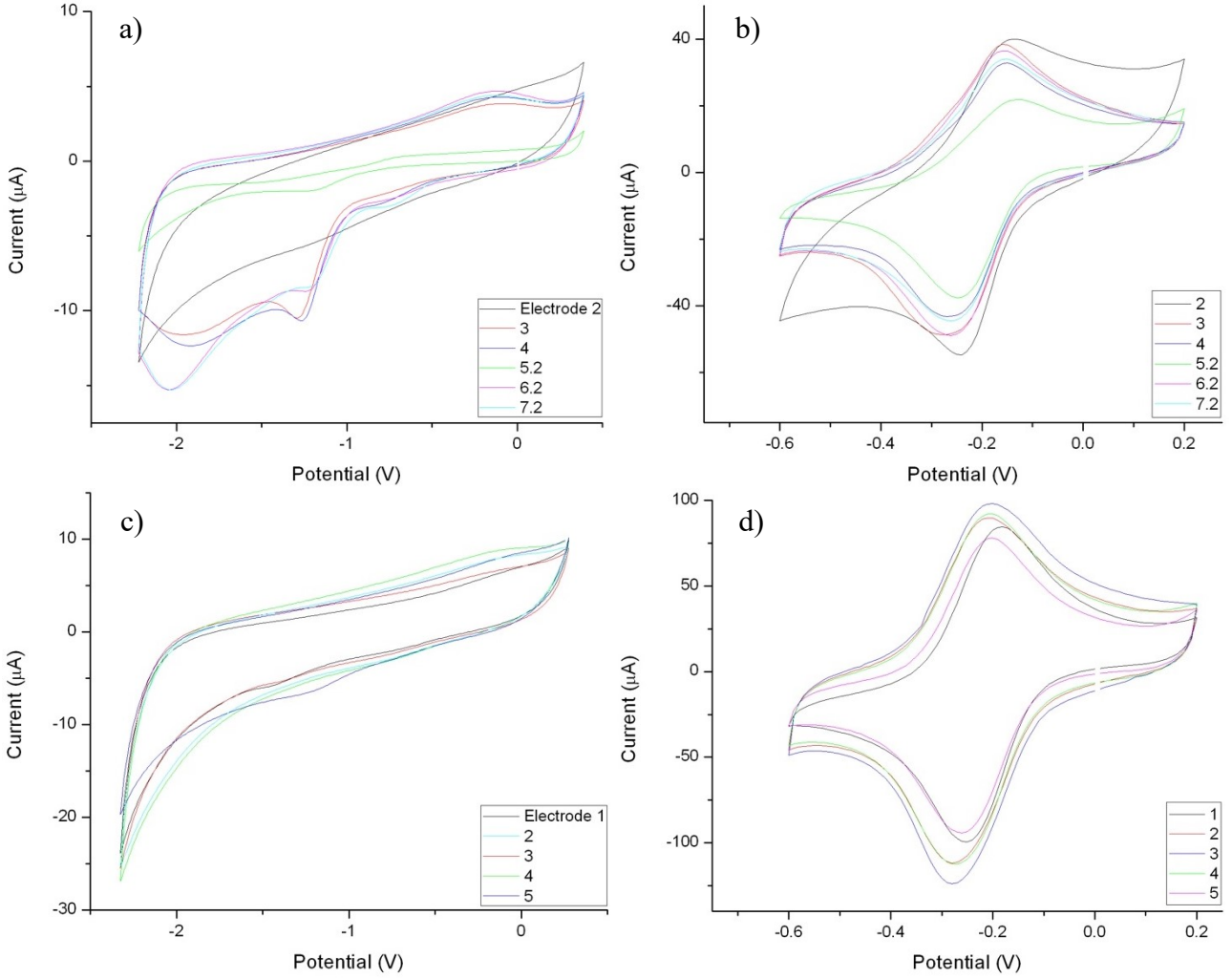


*Figure 8: Reduction and N-doping of nGO done by cyclic voltammetry in 0.1 M LiBF4 in ACN from -2.325 to 0.275 V vs Ag/AgCl wire for 30 cycles with a scan rate of 0.05 V/s with 5 5-µL aliquots of nGO (a) or 17 5-µL aliquots of nGO and annealing for 1 hour at 60°C (c). Characterization of the resulting RNnGO films done by cyclic voltammetry in 1 mM $[Ru(NH_3)_6]Cl_3$ in PBS from -0.6 to +0.2 V vs Ag/AgCl with a scan rate of 0.5 V/s with 5 5-µL aliquots of nGO (b) or 17 5-µL aliquots of nGO and annealing for 1 hour at 60°C (d).*

*Table 2: Calculated surface charge values and the average relative errors for sensors modified with 5 5-µL aliquots of nGO and no annealing compared to 17 5-µL aliquots of nGO and annealing for 1 hour at 60°C.*

| | **5 5-µL aliquots, no annealing** | | **17 5-µL aliquots, 1 hr annealing** | |
|---|---|---|---|---|
| | **Charge (µC)** | **Average relative error (%)** | **Charge (µC)** | **Average relative error (%)** |
| **Reduction and N-doping** | 343 ± 112 | 33 | 469 ± 132 | 28 |
| **RNnGO Characterization** | 27 ± 10 | 36 | 60 ± 13 | 21 |

Reduction is carried out in such a way as to minimize deviations between electrodes. The electrochemical cell is tightly sealed so as to prevent evaporation of the organic solvent, acetonitrile. The electrolyte solution is replaced after each reduction so as to prevent differences between salt concentrations. Despite these precautions, electrodes drop-cast with 5 5-µL aliquots of nGO still show average relative errors of over 30% between electrodes for reduction and N-doping as well as for characterization of the RNnGO film. This irreproducibility can also be seen in the cyclic voltammograms (Figure 8 a.). Extra reduction peaks seen at about -1.25 V for some electrodes are most likely due to oxygen-containing functional groups that have not been fully reduced even after 30 cycles. There is also a factor of 3 difference between the electrode with the lowest calculated charge, electrode 5.2 with 132 µC, and the highest, electrode 7.2 with 435 µC. It can be speculated that the reason for these large deviations in charge may be due to differences in surface roughness of the bare GC electrodes, originating from the electrode polishing step, or simply that the extent of non-conductive nGO converted to conductive RNnGO varies between electrodes. This carefully executed method of reduction and N-doping leads to the conclusion that the error does in fact arise from the drop-casting of nGO prior to reduction and N-doping. By ensuring a quasi-complete coverage of the electrode surface by drop-casting 17 5-µL aliquots and annealing for 1 hour at 60 °C it is possible to attain a more reproducible RNnGO modified electrode. The cyclic voltammograms of the reduction and N-doping shows better reproducibility (Figure 8 c.) with the lack of extra reduction peaks as seen previously in Figure 8 a. The interelectrode reproducibility shows improvement considering the calculated average relative error of the charge capacity is lowered by 15% when characterizing the RNnGO surface. Naturally, with 85 µg of nGO drop-cast on the surface, the total charge capacity of the RNnGO surface becomes much greater due to the increase in electroactive material. The difference is, in fact, calculated as there being over double the charge capacity of RNnGO after drop-casting 17 5-µL aliquots of nGO compared to 5. This can also be seen visually by the difference in amplitude of the peak currents where the maximum values reach 100 µA for the improved drop-casting method compared to only 40 µA for the previous method (Figure 8 b., d.). This improved

method therefore aids in signal amplification of the measured current which will be beneficial for further use of the material in the sensitive and selective detection of cDNA.

### 4.3.3 Effect of N-doping on reduced nGO: comparison of reduction of nGO in propylene carbonate and acetonitrile

To elucidate the effect of N-doping on the electrochemical properties of reduced nanographene oxide (**RnGO**) we reduced a series of electrodes in non-doping solvent, propylene carbonate, and compared their electrochemical characteristics with RNnGO. The electrode characterization was carried out using positively charged redox ions of ferrocene ($Fc/Fc^{+}$) and negatively charged hexacyanoferrate ($[Fe(CN)_6]^{2-/3-}$) to understand if there is partitioning of these ions in the reduced GO due to electrostatic attraction, which can indirectly indicate the surface charge of the films of RnGO and RNnGO.

The nature of cyclic voltammetry is such that the potential is cycled within a potential range causing repeated reduction and oxidation of the redox species at the electrode surface. The information obtained from this method of analysis can provide insight into the electrode material's electrochemical properties as well as the redox process occuring at the electrode surface. When the potential is applied in the positive to negative direction redox species at the electrode surface are reduced and an increase in current is measured as the cathodic peak. As the potential continues in the negative direction, the redox species at the surface become depleted and the measured current diminishes. The point at which the highest current was measured is the anodic peak current. Similarly, when the potential direction is switched from negative to positive, all redox species in the vicinity of the electrode will be oxidized giving a rise in current. In the same manner, the current will peak at the anodic peak current followed by a lowering of current as all redox species are oxidized. Ideally, the products of these reductions and oxidations will be stable enough to allow for the reverse process to occur repeatedly giving rise to anodic and cathodic peaks of the same magnitude. In this case, the ratio of the anodic and cathodic peak currents, $i_{p,a}$ and $i_{p,c}$ respectively, will be close to 1.0 (Equation 5).

$$\frac{i_{p,a}}{i_{p,c}} = 1.0 \tag{5}$$

A reaction is considered irreversible when the product of oxidation and/or reduction is unstable and therefore cannot be reduced or oxidized in the following potential sweep. The peak current ratio will therefore not be equal to 1.0 as the anodic and cathodic peaks will be of different magnitudes.

The potentials at which the peak currents occur provide further information on the reversibility of the electrochemical reaction. The separation of the anodic and cathodic peak potentials, $E_{p,a}$ and $E_{p,c}$ respectively, is given by Equation 6.

$$\Delta E_p = E_{p,a} - E_{p,c} = \frac{58}{n} \quad (6)$$

The potential at which the concentrations of the redox species at the electrode surface are equivalent can be found at the midpoint between the two redox peaks. The formal potential of the redox couple can therefore be determined by Equation 7.

$$E^{\circ\prime} = \frac{E_{p,a}+E_{p,c}}{2} \quad (7)$$

The reversibility of the redox reaction at the electrode surface was compared between bare GC electrodes and the electrodes whose surface was modified with RNnGO and RnGO (Figure 9 and Table 3).

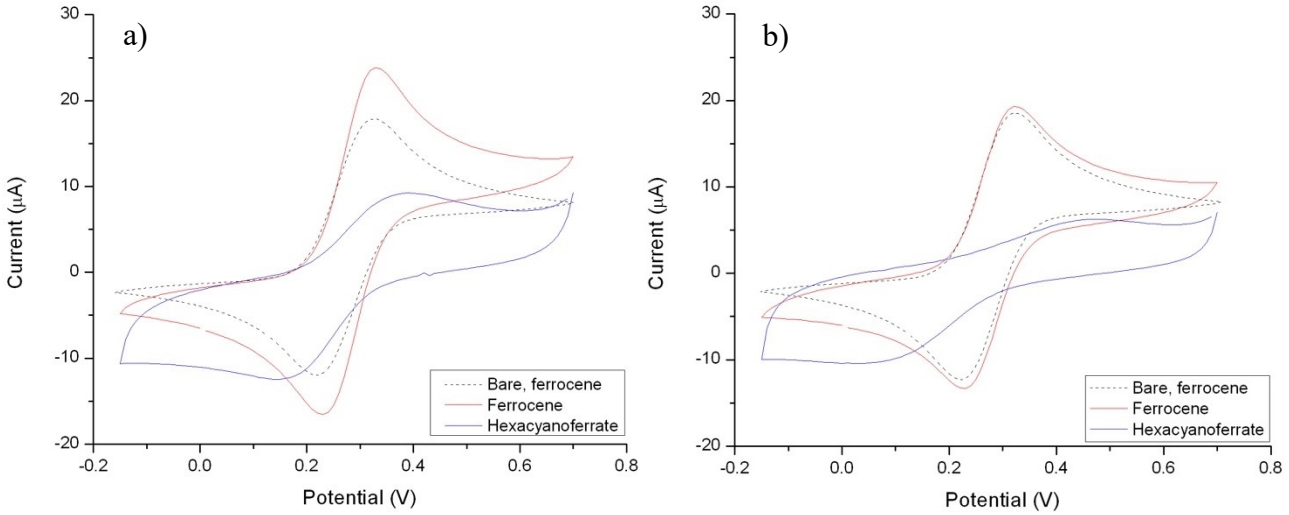


*Figure 9: Comparison of bare, reduced nGO, and reduced and N-doped nGO. Cyclic voltammetry in 1 mM ferrocene in 0.1 M $LiBF_4$ in ACN and in 1 mM hexacyanoferrate in 1.0 M $KNO_3$ from -0.15 to +0.7 V vs Ag/AgCl wire (organic) or Ag/AgCl/3 M KCl (aqueous) with a scan rate of 0.05 V/s. Bare electrodes were conditioned at OCP for 10 minutes before measuring.*

*Table 3: Peak current ratio, peak separation and formal reduction potential calculated for bare, RNnGO and RnGO modified electrodes in the presence of redox couples ferrocene or hexacyanoferrate.*

| **Electrode modification** | **Redox Couple** | $\frac{i_{p,a}}{i_{p,c}}$ | **Peak separation, $\Delta E_p$ (mV)** | **Formal Reduction Potential, $E^\circ$ (mV)** |
|---|---|---|---|---|
| Bare GC | Ferrocene | 1.005 ± 0.004 | 108 ± 8 | 275.6 ± 1.7 |
| RNnGO | Ferrocene | 1.044 ± 0.038 | 104 ± 5 | 274 ± 4 |
| | Hexacyanoferrate | 0.785 ± 0.065 | 176 ± 38 | 270.0 |
| RnGO | Ferrocene | 1,020 ± 0.014 | 90.0 | 283 ± 18 |
| | Hexacyanoferrate | 0.472 ± 0.103 | 366 ± 65 | 259 ± 4 |

All electrodes tested with ferrocene as the redox couple showed good reversibility. The oxidation and reduction peaks can be clearly seen as ferrocene is oxidized to ferrocenium with increasing applied potentials and the reverse process with decreasing applied potentials. However, in the presence of hexacyanoferrate, RNnGO and RnGO both exhibit peak current ratios less than 1.0, RnGO more so than RNnGO. This can be explained by considering the non-uniformity of the films which will influence the redox state of hexacyanoferrate(IV) partitioned within the film. For example, the redox anion can form alternate complexes which will affect its oxidation and reduction potentials or limit its participation in the redox reaction altogether. These effects result in irreversibility of the redox reaction and inferior peak current ratios. The ferrocene/ferrocenium redox reaction has a 1 electron transfer and therefore peak separation should be in the region of 58 mV. The $\Delta E_P$ values for all electrodes in both redox couples were calculated to be significantly larger than 58 mV. The cause for this is most likely due to impurities in deionized water, the paste used for polishing of the GCE and adsorption of organic molecules from the air (Nioradze *et al.,* 2015).

Figure 10 shows that the positive redox couple, ferrocene, has distinctly larger peak currents than the negatively charged redox couple, hexacyanoferrate, thus indicating that N-doped reduced nGO layer on the electrode surface is slightly negatively charged. It therefore repels the negatively charged hexacyanoferrate which hampers its reduction and oxidation at the electrode surface. It is also clear that, compared to RnGO, RNnGO has a 14% and 41% higher peak current when tested in ferrocene and hexacyanoferrate respectively. This can be accounted for by the increased conductivity after modification of the graphene structure by N-doping.

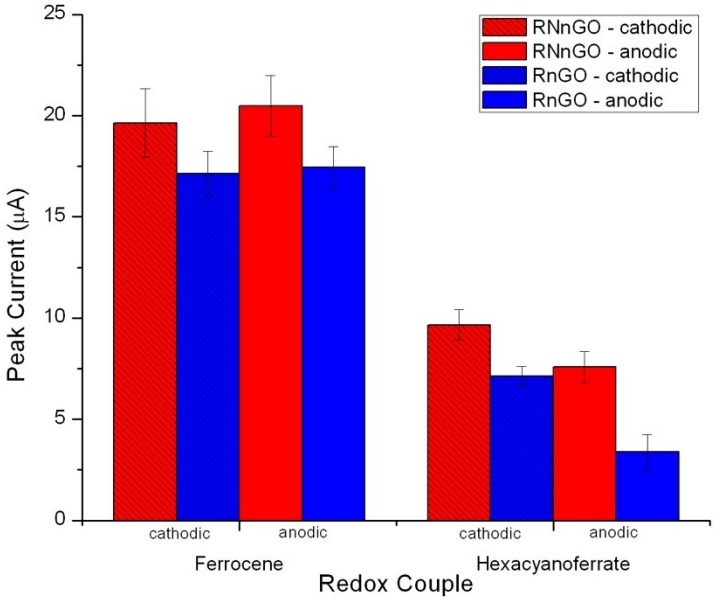


*Figure 10: Anodic and cathodic peak currents measured for RNnGO and RnGO modified electrodes in the presence of a positively charged redox couple, ferrocene, and a negatively charged redox couple, hexacyanoferrate. Peak currents extracted from cyclic voltammograms performed in 1 mM ferrocene in 0.1 M $LiBF_4$ in ACN and in 1 mM hexacyanoferrate in 1.0 M $KNO_3$ from -0.15 to +0.7 V vs Ag/AgCl wire (organic) or Ag/AgCl/3 M KCl (aqueous) with a scan rate of 0.05 V/s.*

Further characterization of the electron transfer kinetics at the electrode surface can be done by varying the scan rate during cyclic voltammetry. An increase in measured current is seen when the standard potential of the redox couple is reached and the reactants in the vicinity of the surface are being reduced or oxidized. Decreasing of the current, and therefore the peak form, is seen when all of the reactant at the surface has been converted and a diffusion layer is formed. The rate of the redox reaction is now controlled by the rate that the reactant diffuses to the electrode, otherwise known as the flux. With a slow scan rate, the diffusion layer grows outwards into the electrolyte solution as more of the reactant is consumed. There is therefore a slower flux of replacing reactant to the surface and the peak currents are low. A fast scan rate means that the diffusion layer does not reach so far and reactant at the surface can be quickly replaced, resulting in a higher flux and increased peak currents.

If the scan rate is increased and the peak potentials remain the same, the electron transfer is considered fast and the redox reaction reversible. In some cases, however, the peak potentials vary as a function of the scan rate; the difference in peak potential increases with increasing scan rates. This is due to a slow electron transfer rate leading to an inability of the redox couple to reach equilibrium and the current response being delayed as the applied potential changes (Figure 11 a., b.). The reduction peaks of RnGO during cyclic voltammetry (Figure 11 b.) are completely overtaken by the faradaic current as the scan rate increases making it impossible to determine the real cathodic peak values.

According the Randles-Sevcik equation, anodic and cathodic peak currents of a reversible redox reaction will have a linear variance in respect to the square root of the scan rate. Peak currents that do not vary linearly with the square root of the scan rate are considered to be from an irreversible or quasi-reversible redox reaction. Figure 11 c., d. shows that the reduction peak currents increase linearly with increasing scan rates, however, oxidation peak currents do not. A linear correlation points to the reduction reaction being diffusion controlled as the double layer thickness is modified depending on the scan rate. The plateau seen for the oxidation peak correlation may be an effect of the negatively charged surface and the electrostatic repulsion submitted to hexacyanoferrate.

Figure 11 e., f. shows that the peak current ratio decreases while the peak separation increases with increasing scan rate for both RnGO and RNnGO. This is further proof towards the irreversibility of the redox reaction occurring at the electrode surface.

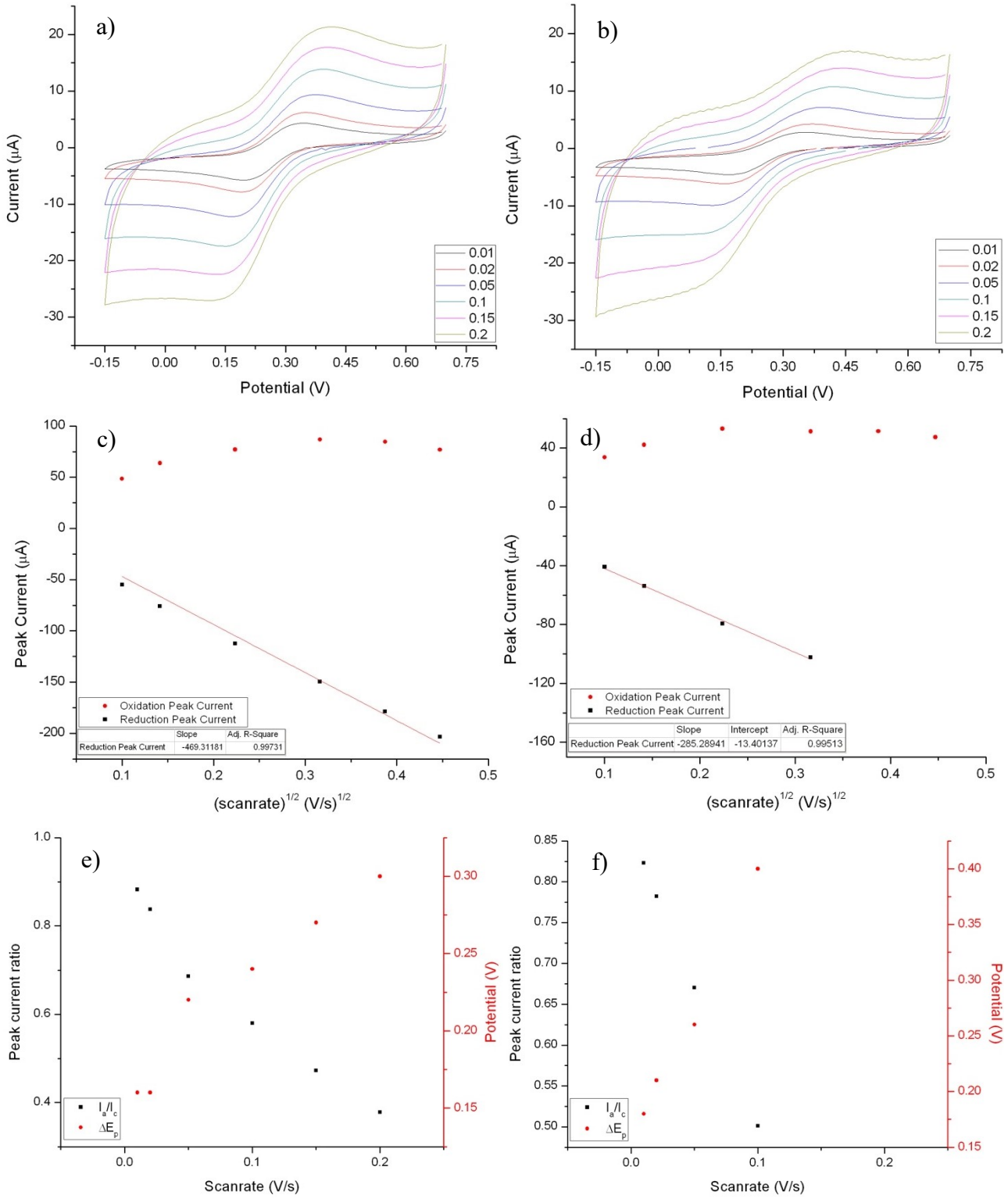


*Figure 11: Dependence of peak current and peak separation on scan rate for RNnGO (a., c., e.) and RnGO (b., d., f.) Cyclic voltammetry performed in 1 mM $K_3Fe(CN)_6$ in 0.1M $KNO_3$ from -0.15 to 0.7 V vs Ag/AgCl/3 M KCl at scan rates varying from 0.01 to 0.2 V/s.*

### 4.3.4 Characterization by EIS

Electrochemical impedance spectroscopy (**EIS**) is a useful analytical technique as it is able to provide information on the electrical impedance of complex set of components and interfaces within a system. The principle is to apply an excitation signal at a set of given frequencies and measure the resulting current signal which is representative of the rate of the electrochemical reaction. As the excitation signal is applied, it interacts with the system and undergoes a phase shift which is detected as a delay in the response and is dependent on the frequency. The impedance ($Z$) is expressed in a Nyquist plot of the imaginary impedance ($-Z''$) as a function of the real impedance ($Z'$). The obtained data can be related to the electrochemical reactions occurring at the electrode/electrolyte interfaces The system can therefore be defined by an equivalent circuit containing electrical components such as a resistor, capacitor or impedance. Resistors can results from electron transfer between two materials, results in a measurable charge-transfer resistance, or from the resistance of the electrolyte solution. Capacitors can arise from the charging of the electrical double layer at the interface between the electrode and the bulk solution. Impedance elements, such as Warburg impedance, tangential and cotangential hyperbolic element, result from the diffusion of reactants within the system to either infinite or finite distances.

In the case of a bare electrode modified with RNnGO or RnGO, it is possible to perform EIS to obtain information on the capacitive properties of each material. Capacitance is an important characteristic of graphene-based materials as it defines the material's ability to store charge. Nyquist plots obtained by performing EIS of electrodes modified with either RNnGO or RnGO are compared to a bare GC electrode (Figure 12).

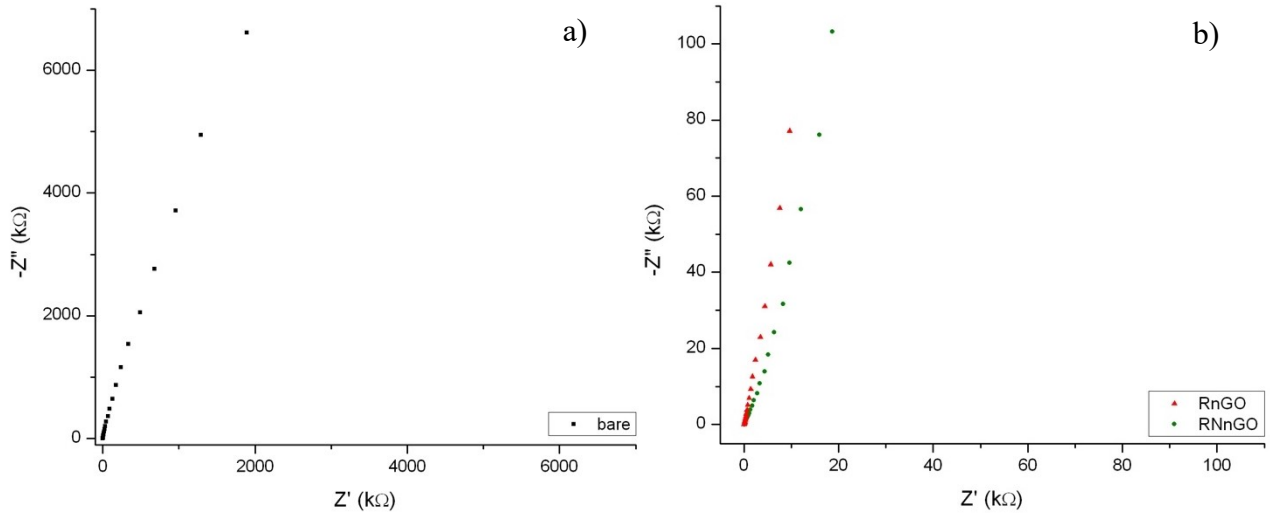


*Figure 12: Nyquist plots for bare electrode (a.) nGO reduced (RnGO) and nGO reduced and N-doped (RNnGO) (b,). EIS was performed in 50 mM PBS (I=0.5 M, pH 7.0), at OCP from 100 kHz to 0.01 Hz.*

For the impedance spectra of the bare electrodes and the electrodes modified with RNnGO and RnGO it was impossible to obtain good fit using standard models (Randles equivalent circuit and Randles equivalent circuit modified with Warburg impedance) having sensible electrochemical meaning. The EIS analysis is therefore has been limited to extracting the values of *-Z''* at the lowest frequency, in this case 10 mHz, in order to calculate capacitance for each material using equation 8 where *C* is the capacitance, *f* is the frequency and *-Z''* is the imaginary impedance (Table 4) (Österholm *et al.*, 2012).

$$C = \frac{1}{2\pi f|-Z''|} \tag{8}$$

*Table 4: Capacitance values calculated from extracted -Z'' values from EIS data at the lowest frequency for bare, RNnGO and RnGO electrodes.*

| Electrode modification | C (μF) |
|---|---|
| Bare | 2.28 ± 0.41 |
| RNnGO | 168.75 ± 14.72 |
| RnGO | 207.79 ± 12.62 |

As seen from the table, the bare GC electrode would have the lowest capacitance compared to the electrodes modified with graphene derivatives. This is most probably due to the increased surface area of the electrode caused by corrugated shape of reduced graphene oxide flakes. The double layer capacitance of N-doped reduced nGO is slightly lower compared to reduced nGO although is in the same order of magnitude. The reason of this we don't know as it would require finding the optimal equivalent circuit to describe the electrochemical behaviour of these electrodes and finding the values of pseudocapacitance introduced by N atoms, which is out of scope of this work.

### 4.3.5 Dissolution of RNnGO in aqueous media

After reduction and N-doping of nGO, further modifications and characterizations of the DNA-selective biosensor are done in aqueous media. It is therefore important to identify whether RNnGO is soluble in aqueous solutions and how its electrochemical performance can degrade over time due to its dissolution. The electrode modified with RNnGO was therefore tested in PBS by cyclic voltammetry to see how fast and if its surface charge deteriorates within 100 cycles of the analysis (Figure 13). By integration of the CVs current over the time, it can be determined that, between the 2$^{nd}$ and 100$^{th}$ cycle, there is only a 3.3% loss of charge capacity (Table 5). RNnGO can consequently

be defined as insoluble in aqueous media and electrochemically stable within the chosen window of the potentials to the extent that shall not compromise the biosensor performance.

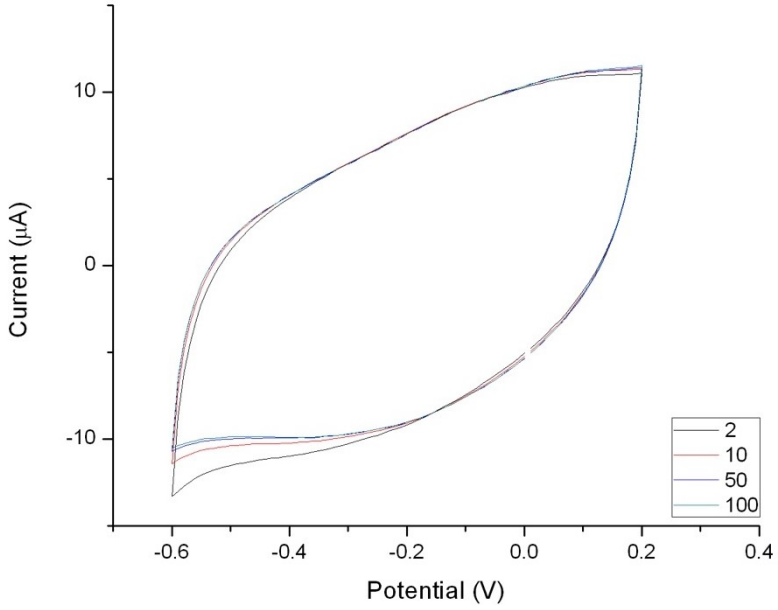


*Figure 13: Test for dissolution of reduced, N-doped nGO in aqueous media over 100 cycles. Cyclic voltammetry in 50 mM PBS (I=0.5 M, pH 7.0) from -0.6 to +0.2 V with a scan rate of 0.1 V/s. Shown are cycles 2, 10, 50 and 100.*

*Table 5: Integrated areas of CVs representing charge capacity of the electrode surface.*

| Cycle | Charge (µC) |
|---|---|
| 2 | 121.93 |
| 10 | 119.15 |
| 50 | 117.95 |
| 100 | 117.89 |

## 4.4 Application of RNnGO in DNA biosensor

### 4.4.1 Immobilization of DNA probe

The RNnGO material was used in fabricating of a DNA biosensor in order to attain a higher success rate of cDNA hybridization. Both the amount of drop-cast nGO and the reduction potential were optimized with the objective of immobilizing DNA probe that could successfully hybridize with cDNA. The DNA probe is crosslinked to the surface through covalent bonds between the thiol group of the DNA probe and the crosslinker's maleimide group. Concurrently, the crosslinker's ester group forms covalent bonds with the amine groups present within the RNnGO material. Therefore, the density of amines within the RNnGO material will determine the density of DNA probe crosslinked to the surface. The surface coverage of RNnGO also has an effect on the amount of immobilized

DNA probe; a higher area of RNnGO results in a higher number of N-atoms inserted into the graphene lattice which are available for crosslinking.

The effect of the amount of drop-cast nGO on immobilization of the DNA probe can be seen in Figure 14. The sensors were characterized by cyclic voltammetry in the presence of $[Ru(NH_3)_6]Cl_3$ after reduction and N-doping of nGO as well as after immobilization of the DNA probe. The reduction and oxidation of $[Ru(NH_3)_6]^{3+/2+}$ at the unmodified RNnGO surface is solely due to the electron transfer of the redox couple in the electrolyte solution. After immobilization of the DNA probe, however, $[Ru(NH_3)_6]^{3+}$ becomes incorporated into the DNA backbone due to the ion exchange between the redox cations and $Na^+$. This addition of excess redox couple to the electrode film results in an increase in the electrochemical signal and a higher measured charge compared to the unmodified RNnGO.

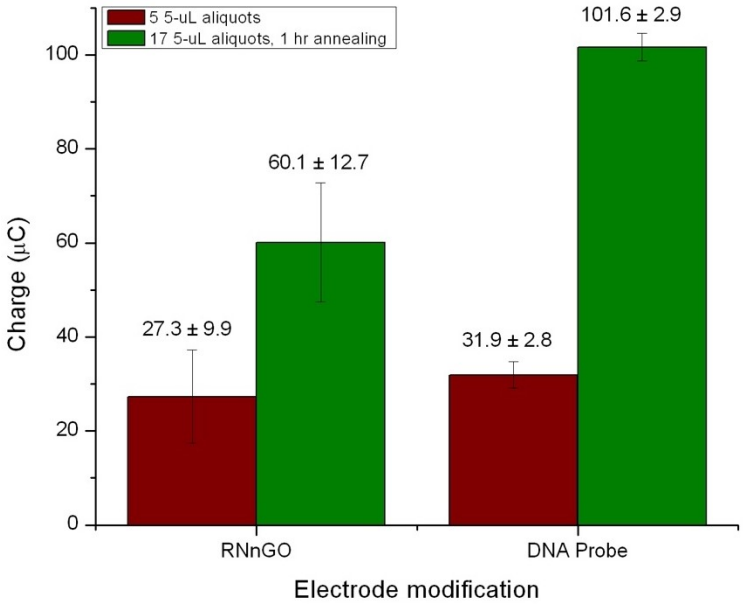


*Figure 14: The effect of amount of drop-cast nGO on DNA probe immobilization. Calculated surface charge from cyclic voltammograms performed after reduction and N-doping of nGO and after subsequent DNA probe immobilization in 1 mM $[Ru(NH_3)_6]Cl_3$ in PBS from -0.6 to +0.2 V vs Ag/AgCl with a scan rate of 0.5 V/s.*

A sensor modified with only 5 5-µL aliquots of nGO shows a 17% increase in surface charge from RNnGO to after probe immobilization. In comparison, a sensor modified with 17 5-µL aliquots shows a 69% increase in surface charge. The fact that the optimized RNnGO material exhibits such a high increase in surface charge shows that the increased surface coverage aids in a more effective immobilization of the DNA probe.

### 4.4.2 Blocking

The DNA probe is only immobilized through crosslinking to the amines present within the RNnGO surface. Therefore, any bare spots or unreacted sites on the surface become target to non-specific adsorption of DNA present within the sample solution. This non-specific adsorption leads to the detection of DNA in the sample even if it is not target DNA and not complementary to the DNA probe. As it would result in false positive results, it is crucial that a blocking technique is employed to cover bare spots at the electrode surface. Bovine serum albumin (**BSA**) is a small and unreactive protein which is able to block nonspecific binding sites. Calf thymus DNA (**CT-DNA**) does the same, however, due to its long and mobile form, it is able to better conform to the surface and result in improved blocking of bare spots. Therefore, both BSA and CT-DNA were compared as electrode surface blocking techniques and their effect on DNA selectivity was assessed. Sensors blocked with either BSA or CT-DNA were tested for cDNA selectivity by performing cyclic voltammetry in the presence of $[Ru(NH_3)_6]Cl_3$ after DNA probe immobilization, after incubation in ncDNA and after incubation in cDNA. The DNA surface densities were calculated for each experimental procedure in order to determine whether the sensors exhibited DNA selectivity and measured a higher DNA surface density for cDNA versus ncDNA (Figure 15).

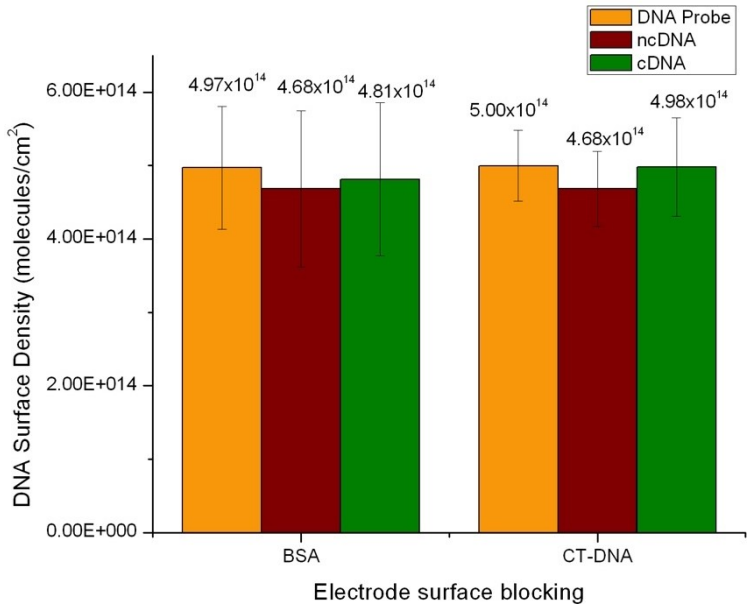


*Figure 15: Comparison between blocking the electrode surface with BSA versus CT-DNA. Calculated DNA surface density from cyclic voltammograms taken after probe immobilization, after ncDNA incubation and after cDNA incubation.*

When measuring the positive difference in signal between ncDNA and cDNA, blocking with CT-DNA resulted in a difference of (5.82 ± 3.63) $x10^{13}$ molecules/$cm^2$ in DNA surface density compared to (2.00 ± 0.49) $x10^{13}$ molecules/$cm^2$ when the bare spots on the electrode surface were blocked with BSA. It should be noted that the DNA surface density after immobilization of the DNA probe is consistently greater than after hybridization with cDNA. This is contradictory to what one

might expect considering that there should be a larger amount of $[Ru(NH_3)_6]^{3+}$ intercalated within the strands of dsDNA compared to ssDNA. The explanation for this is unknown, however, it has been chosen to define a positive hybridization event as a greater DNA surface density after incubation in cDNA compared to ncDNA. The rate of false positive responses between electrodes was also shown to improve when comparing the standard deviations of the two blocking methods: circa 20% of the electrodes blocked with BSA were rejected based on false positive response versus 11% for the electrodes blocked with CT-DNA. CT-DNA was therefore chosen as the blocking molecule to be used for our DNA biosensors.

### 4.4.3 Sensing

The optimized biosensors, modified with 17 aliquots of nGO that was then converted to RNnGO, DNA probe and blocked with CT-DNA, were tested for selectivity towards cDNA and compared to the previous iteration before optimization (Figure 16).

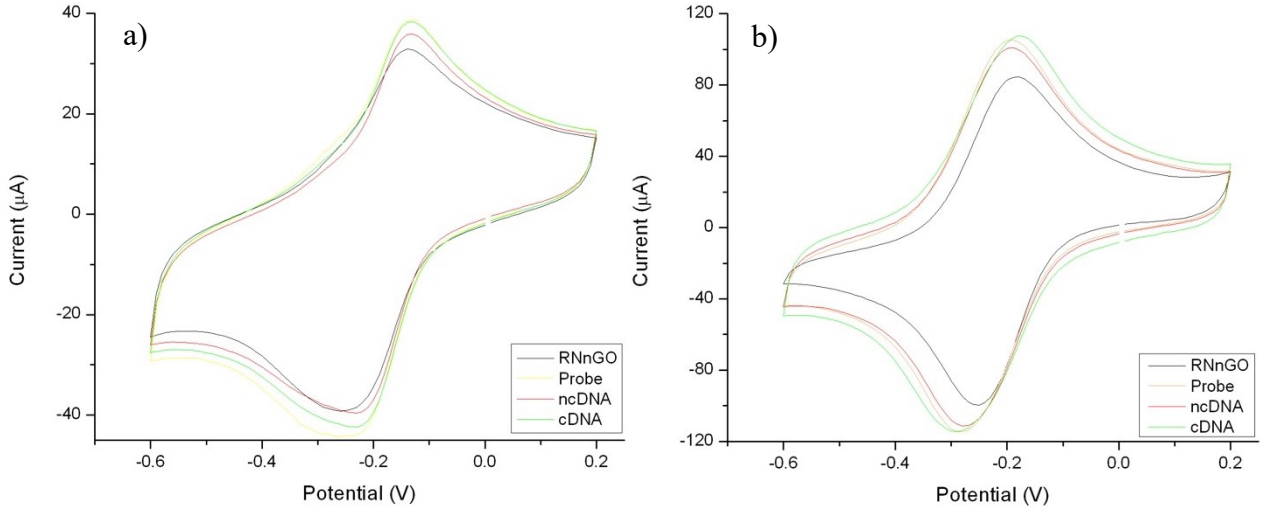


*Figure 16: Cyclic voltammetric responses of RNnGO modified sensors with (a) 5 5-µL aliquots of nGO and (b) 17 5-µL aliquots of nGO with 1 hour annealing. Electrode characterizations were carried out after N-doping and reduction, probe immobilization, incubation in ncDNA and incubation in cDNA. Cyclic voltammetry was performed in 1 mM $[Ru(NH_3)_6]Cl_3$ in PBS from -0.6 to +0.2 V vs Ag/AgCl/3 M KCl with a scan rate of 0.5 V/s.*

It can be seen from the CVs that the measured current amplitude is greatly increased for 17 5-µL aliquots of nGO compared to 5 5-µL aliquots due to the increased amount of electrochemically active RNnGO present on the surface. While Figure 16 a. exhibits CVs that are generally overlapping despite modifications with DNA, the CVs in Figure 16 b. are easily discerned between the bare RNnGO surface and after probe immobilization. In addition, the optimized sensors show well defined and symmetrical anodic and cathodic redox peaks compared to the previous sensors that show a widened cathodic peak compared to the anodic peak. The DNA surface densities were obtained from

integration of the CVs recorded after probe immobilization, after incubation in ncDNA and after incubation in cDNA (Figure 17).

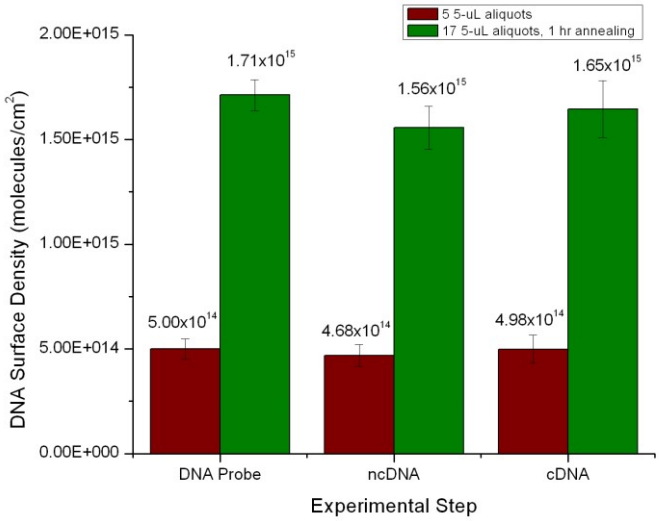


*Figure 17: The effect of electrode surface modification on DNA biosensor performance. Calculated DNA surface density from cyclic voltammograms taken after probe immobilization, after incubation in ncDNA and cDNA.*

Of the optimized electrodes tested, 100% showed selectivity towards cDNA compared to 73% for electrodes cast with 5 5-µL aliquots of nGO. The average positive response amplitude also increased from $(5.82 \pm 3.63)\text{x}10^{13}$ molecule/cm$^2$ to $(8.95 \pm 7.21)\text{x}10^{13}$ molecule/cm$^2$. The optimized method for modification of GC electrode with RNnGO and DNA probe is therefore favourable for the development of a DNA biosensor with improved selectivity for target DNA.

### 4.4.4 Characterization of DNA modification by EIS

As an alternative sensing approach, EIS measurements were done after each surface modification step with DNA in order to detect changes in the electrical properties of the sensor components that would elucidate successful DNA hybridization. A typical Nyquist plot for a DNA modified biosensor after immobilization of the DNA probe, after incubation in ncDNA and after incubation in cDNA is shown in Figure 18.

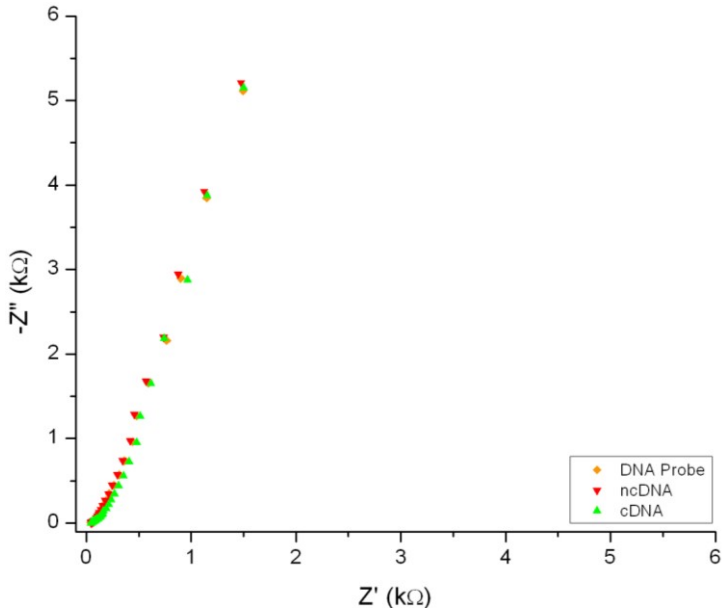


*Figure 18: Nyquist plot for a DNA biosensor after DNA probe immobilization, after incubation in ncDNA and after incubation in cDNA. EIS was performed in 1 mM $[Ru(NH_3)_6]Cl_3$ in 50 mM PBS (I = 0.5 M, pH 7.0) at OCP from 100 kHz to 0.1 Hz.*

The plot can be characterized by a linear line extending across the range of frequencies indicating that the majority of the process is diffusion controlled. As noted by Bobacka *et al.*, 1999, the lack of a semicircle in the high frequency region of the impedance spectra points to fast electron transfer kinetics. This can be accounted for by the fact that the redox couple, $[Ru(NH_3)_6]^{3+}$, is electrostatically bound to the negatively charged backbones of the immobilized DNA. Charge transfer due to the redox couple therefore occurs directly at the electrode surface. With increasing DNA present with successful hybridization, the amount of $[Ru(NH_3)_6]^{3+}$ will increase proportionately and the charge transfer resistance will decrease further due to the facilitated electron transfer. Considering that the DNA and $[Ru(NH_3)_6]^{3+}$ will form a self-assembly monolayer between the electrode surface and the surrounding electrolyte, the DNA component can be represented by a constant phase element, *CPE*, in the equivalent circuit (Figure 19).

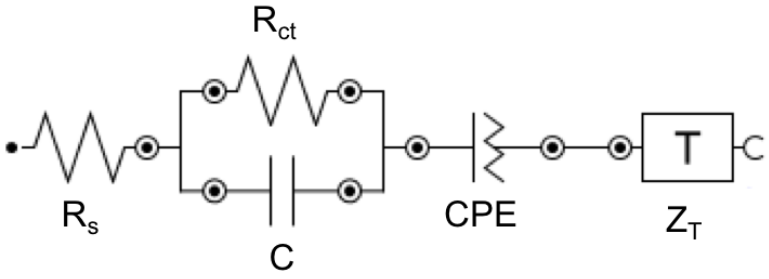


*Figure 19: Equivalent circuit of a DNA biosensor.*

A constant phase element is considered a non-ideal capacitor and is therefore defined by $Y_0$, which is relative to the capacitance, and $N$, which is an exponent that can vary between 0 and 1 for an ideal resistor and an ideal capacitor respectively. Additional components of the equivalent circuit

include, $R_s$, the resistance of the electrolyte solution (1 mM $Ru(NH_3)_6]Cl_3$ and 50 mM PBS) and $R_{ct}$ and $C$ in parallel pertaining to RNnGO as it partakes in both the electron transfer as well as the formation of a double layer between the RNnGO material and the immobilized DNA probe. Finally, $Z_T$ is known as the finite Warburg impedance which represents the frequency dependent diffusion of ions in the bulk. The diffusion length is considered finite in order to account for the shift from the 45° phase angle to a 90° capacitive line. As the $[Ru(NH_3)_6]^{3+}$ cations can exchange $Na^+$ in DNA molecule at 20 different phosphate groups their diffusion within the monolayer can be therefore described with finite length diffusion element T. The obtained EIS data was fit to the equivalent circuit using the software NOVA 1.11 and the resulting values for each electrical component are listed in Table 6.

*Table 6: Resistance ($R_s$ and $R_{ct}$), capacitance (C), constant phase element variables (CPE $Y_0$, CPE N) and the finite Warburg impedance variables ($Z_T$ $Y_0$ and $Z_T$ N) obtained after fitting of the EIS data to the equivalent circuit (Figure 19), n = 5*

| **Experimental Step** | **Sensor modification** | **$R_s$ (Ω)** | **$R_{ct}$ (kΩ)** | **C (mF)** | **CPE: $Y_0$ ($mΩ^{-1}$)** | **CPE: N** | **$Z_T$: $Y_0$ ($mΩ^{-1}$)** | **$Z_T$: B** | **$X^2$** |
|---|---|---|---|---|---|---|---|---|---|
| 5 5-mL aliquots nGO | DNA Probe | 50.41 ± 0 | 1.86 ± 0.13 | 258.43 ± 0.11 | 0.17 ± 0.05 | 0.86 ± 0.03 | 2.12 ± 0.16 | 10.79 ± 0 | 0.14 ± 0.12 |
| | ncDNA | 52.63 ± 0 | 1.33 ± 0.13 | 317.52 ± 0.10 | 0.14 ± 0.03 | 0.78 ± 0.01 | 3.01 ± 0.21 | 10.82 ± 0 | 0.09 ± 0.10 |
| | cDNA | 53.06 ± 0 | 1.75 ± 0.13 | 423.37 ± 0.08 | 0.14 ± 0.02 | 0.76 ± 0.01 | 2.26 ± 0.14 | 10.76 ± 0 | 0.05 ± 0.07 |
| 17 5-mL aliquots nGO, 1 hr annealing | DNA Probe | 33.46 ± 0 | 41.73 ± 0.08 | 357.01 ± 0.01 | 26.39 ± 0.06 | 0.14 ± 0.07 | 1.65 ± 0.02 | 10.73 ± 0 | 0.02 ± 0.02 |
| | ncDNA | 35.06 ± 0 | 37.38 ± 0.06 | 337.34 ± 0.01 | 35.60 ± 0.07 | 0.14 ± 0.09 | 1.72 ± 0.02 | 10.73 ± 0 | 0.02 ± 0.02 |
| | cDNA | 34.48 ± 0 | 40.12 ± 0.06 | 340.94 ± 0.01 | 25.58 ± 0.06 | 0.17 ± 0.04 | 1.72 ± 0.05 | 9.99 ± 0 | 0.01 ± 0.01 |

The effect of the immobilization of DNA probe and cDNA hybridization on EIS measurements was compared between DNA biosensors modified with 5 5-µL aliquots of nGO and 17 5-µL aliquots of nGO. The fitting was performed in such a way so as to minimize the fitting error,

$X^2$, where 67% and 100% of the fittings for 5 5-µL aliquots of nGO and 17 5-µL aliquots respectively were of the order of magnitude of $10^{-2}$. However, on average, there was still a considerable deviation in error between electrodes as seen in the standard deviation of $X^2$. Despite this, it is still believed that the chosen equivalent circuit best represents the materials with which the DNA biosensor is modified.

The resistance of the electrolyte solution, $R_s$, is considered constant throughout considering that all EIS measurements were done in similar conditions. The increase of one order of magnitude in $R_{ct}$ from electrodes modified with 5 5-µL aliquots of nGO to 17 5-µL aliquots of nGO can be accounted for by the increase of surface coverage of RNnGO as there would be no bare GC exposed to the electrolyte solution for direct electron transfer. While the $Y_0$ of the CPE element cannot be directly related to the capacitance of the DNA modified surface, it is interesting to note that, between 5 5-µL aliquots of nGO to 17 5-µL aliquots of nGO, there is a difference of $10^2$ which may be due to the increased surface density of immobilized DNA probe. While it is possible to obtain some explanations for the physical parameters analyzed, limitations from the analytical software do not permit the determination of parameters that would aid in detecting successful cDNA hybridization. An alternate experimental design would therefore be beneficial in obtaining a deeper understanding of the electrochemical processes occurring within the system. EIS performed in the presence of a negatively charged redox couple, such as $[Fe(CN)_6]^{3-}$, would have the opposite effect on the charge transfer resistance compared to $[Ru(NH_3)_6]^{3+}$. Increasing amounts of DNA present at the surface would cause an accumulation of negative charge which would repel $[Fe(CN)_6]^{3-}$ from the surface. Successful cDNA hybridization would therefore result in increased charge transfer resistance and the manifestation of a large semicircle in the Nyquist plot (Benvidi *et al.,* 2014).

### 4.4.5 Reusability

The reusability of the DNA biosensor can be determined by comparing the response to cDNA after the initial electrode modification to that after denaturation has been performed. The desired result would be that denaturation would separate the hybridized cDNA from the DNA probe which would be left intact on the electrode surface. Three different denaturation methods were tested: heating at 57°C for 15 minutes, at 70°C for 20 minutes and by incubation in 1M NaOH for 1 minute at room temperature (Figure 20).

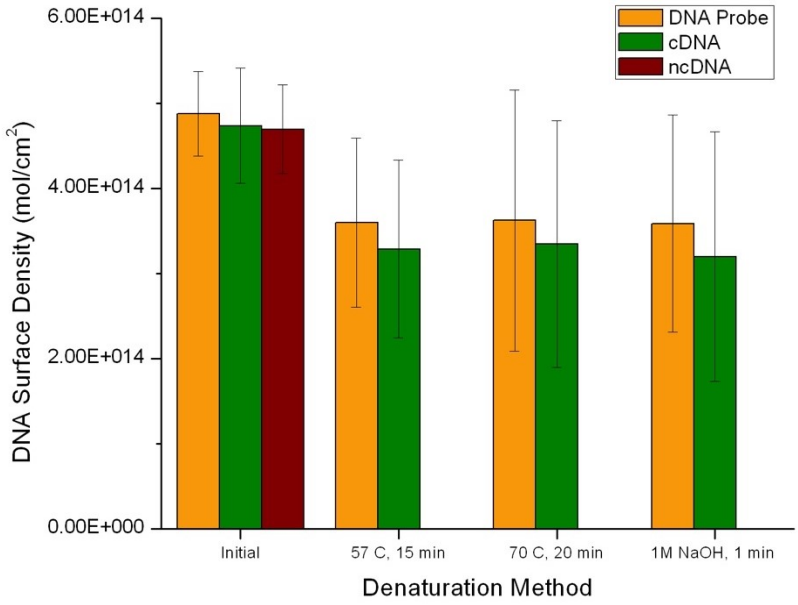


*Figure 20: Change in DNA surface density initially and after various denaturation methods. Electrodes were characterized after denaturation and after incubation in cDNA by cyclic voltammetry in 1 mM $[Ru(NH_3)_6]Cl_3$ in PBS from -0.6 to +0.2 V vs Ag/AgCl/3 M KCl with a scan rate of 0.5 V/s.*

It can be seen that after the first denaturation process, the surface density of DNA probe dropped by 26% and stayed about the same after subsequent denaturation procedures. Compared to the initial response to cDNA versus probe DNA, the following responses to cDNA were much lower. While further experimentation and analysis by fluorescence scanning could be pursued, it was chosen to proclaim these DNA biosensors as single-use.

# 5. Conclusion

The current work outlines the scientific research completed with the objective of improving the methods used to prepare electrochemically reduced and N-doped nGO with a direct application in DNA biosensing. The factors for irreproducibility in the RNnGO films were identified and measures were taken to improve the properties of the resulting films.

The initial electrochemical surface areas of the bare GC electrodes were measured by performing cyclic voltammetry at different scan rates and determining the variance of peak current as a function of scan rate. By using the Randles-Sevcik equation, the electrochemical surface areas were calculated to be (0.056±0.002) $cm^2$. It was determined that the main source of error in preparation of RNnGO films resulted from irreproducibility in the drop-casting method and therefore the total coverage of the electrode surface. A thorough approach was therefore applied to the drop-casting method and a maximum coverage of nGO on the GC electrode surface was reached after casting 17 5-µL aliquots of nGO. Further improvement of the surface coverage was achieved by thermal annealing of the drop-cast electrodes for 1 hour at 60°C. The resulting material was examined by SEM which showed changes in the surface morphology congruent with extensive drying of the nGO film . The insolubility of nGO in organic solvents was verified before continuing with its reduction in acetonitrile. The optimized drop-casting procedure reduced deviations in the RNnGO films by 15% and increased the charge capacity over double.

A series of window of potentials of nGO were tested in order to determine the optimum extent of reduction and N-doping in order to achieve a DNA biosensor with a rate of successful cDNA detection. Electrodes modified with nGO were reduced and N-doped by cyclic voltammetry with potentials ranging from +0.385 to -2.6 V *vs* Ag/AgCl/3 M KCl. The resulting RNnGO electrodes were modified with probe DNA and their selectivity towards cDNA assessed. Out of the potential windows assayed, -2.215 to +0.385 V resulted in a 73% success rate and the highest signal amplitude for cDNA detection.

N-doping of reduced nGO, compared to simply reduced nGO, was determined to create an overall negative charge of the electrode surface made apparent by the difference in peak currents of cyclic voltammograms performed in oppositely charged redox probes. The negatively charged surface promotes reversibility of the redox reaction for positive redox couples demonstrated by a peak current ratio equal to 1.0. Conversely, the electrostatic repulsion of negatively charged redox couples resulted in electron transfer kinetics indicative of an irreversible redox reaction at the electrode surface: peak current ratios less than 1.0 and nonlinearity of peak currents as a function of scan rate.

Characterization of RNnGO films by EIS demonstrated lower capacitive properties compared to RnGO.

Finally, the optimized modification procedure for RNnGO films was applied in the preparation of DNA biosensors. The improved method resulted in a 69% increase in measured surface charge after immobilization of DNA probe compared to 17% with the previous method. The rate of successful cDNA detection also increased to 100% while the positive single amplification increased by a factor of 1.5. Characterization of DNA hybridization was attempted by EIS, however, further research is required in order to perfect the experimental conditions and analytical technique.

The method outlined above for the preparation of DNA biosensors based on RNnGO films succeeded in improving the reproducibility of the RNnGO product as well as improving the performance of the sensor in selectively hybridizing cDNA. There are, however, still advances to be made in the preparation and characterization of the RNnGO films in order fully tailor them to the application in DNA biosensors. The detection of DNA by electrochemical methods is by its very nature at the frontier of medical diagnostics. Consequently, there is still a requirement for a complete understanding of the underlying mechanisms of the electrochemical detection of DNA before DNA biosensors reach real medical applications.

# 6. References

Ambrosi, A., Chua, C. K., Latiff, N. M., Loo, A. H., Wong, C. H. A., Eng, A. Y. S., … Pumera, M. (2016). Graphene and its electrochemistry – an update. *Chem. Soc. Rev.*, *45*(9), 2458–2493.

Benvidi, A., Rajabzadeh, N., & Mazloum-ardakani, M. (2014). Biosensors and Bioelectronics Simple and label-free electrochemical impedance Amelogenin gene hybridization biosensing based on reduced graphene oxide. *Biosensors and Bioelectronic*, *58*, 145–152.

Bobacka, J., Lewenstam, A., Ivaska, A., & Fin, A. (2000). Electrochemical impedance spectroscopy of oxidized poly ( 3 , 4-ethylenedioxythiophene ) film electrodes in aqueous solutions. *Journal of Electroanalytical Chemistry*, *489*, 17–27.

Boukhvalov, D. W., & Katsnelson, M. I. (2008). Modeling of Graphite Oxide. *J. Am. Chem. Soc.*, *8*(15), 10697–10701.

Chen, W., Chen, S., Dong, C. Q., Xing, Y. G., & Wee, A. T. S. (2007). Surface transfer p-type doping of epitaxial graphene. *Journal of the American Chemical Society*, *129*(34), 10418–10422.

Cohen-Tanugi, D., & Grossman, J. C. (2012). Water desalination across nanoporous graphene. *Nano Letters*, *12*(7), 3602–3608.

Deng, D., Pan, X., Yu, L., Cui, Y., Jiang, Y., Qi, J., … Bao, X. (2011). Toward N-doped graphene via solvothermal synthesis. *Chemistry of Materials*, *23*(5), 1188–1193.

Devanathan, R., Chase-woods, D., Shin, Y., & Gotthold, D. W. (2016). Molecular Dynamics Simulations Reveal that Water Diffusion between Graphene Oxide Layers is Slow. *Nature Scientific Reports*, (April), 1–8.

Dreyer, D. R., Park, S., Bielawski, W., & Ruoff, R. S. (2010). The chemistry of graphene oxide. *Chem. Soc. Rev.*

Dubonos, S. V., Grigorieva, I. V., Novoselov, K. S., Morozov, S. V., Firsov, A. A., Geim, A. K., … Jiang, D. (2005). Two-dimensional gas of massless Dirac fermions in graphene. *Nature*, *438*(7065), 197–200.

Geim, A. K., & Novoselov, K. S. (2007). The rise of graphene. *Nature Materials*, *6*, 183–191.

Giovannetti, G., Khomyakov, P. A., Brocks, G., Karpan, V. M., Van Den Brink, J., & Kelly, P. J. (2008). Doping graphene with metal contacts. *Physical Review Letters*, *101*(2), 4–7.

Guo, H., Wang, X., Qian, Q., Wang, F., & Xia, X. (2009). A Green Approach to the Synthesis of Graphene Nanosheets. *ACS Nano*, *3*(9), 2653–2659.

Hammond, J. L., Formisano, N., Estrela, P., Carrara, S., & Tkac, J. (2016). Electrochemical biosensors and nanobiosensors. *Essays in Biochemistry*, *60*, 69–80.

Huang, L., Wu, B., Chen, J., Xue, Y., Geng, D., Guo, Y., … Liu, Y. (2013). Gram-scale synthesis of graphene sheets by a catalytic arc-discharge method. *Small*, *9*(8), 1330–1335.

Hui, K. H., Ambrosi, A., Pumera, M., & Bonanni, A. (2016). Improving the Analytical Performance of Graphene Oxide towards the Assessment of Polyphenols. *Chem. Eur. J.*, *22*, 3830–3834.

Hummers, W. S., & Offeman, R. E. (1958). Preparation of Graphitic Oxide. *Journal of the American Chemical Society*, *80*(6), 1339.

Jiang, D., Cooper, V. R., & Dai, S. (2009). Porous graphene as the ultimate membrane for gas separation-Supplementary Materials. *Nano Letters*, *9*(12).

Kwon, O. S., Park, S. J., Hong, J., Han, A., Lee, J. S., & Lee, J. S. (2012). Flexible FET-Type VEGF Aptasensor Based on Nitrogen-Doped Graphene Converted from Conducting Polymer. *American Chemical Society Nano*, *6*(2), 1486–1493.

Li, X., Wang, H., Robinson, J. T., Sanchez, H., Diankov, G., & Dai, H. (2009). Simultaneous Nitrogen Doping and Reduction of Graphene Oxide. *J. Am. Chem. Soc.*, *131*(43), 15939–15944.

Li, Y., Wang, P., Wang, L., & Lin, X. (2007). Overoxidized polypyrrole film directed single-walled carbon nanotubes immobilization on glassy carbon electrode and its sensing applications. *Biosensors and Bioelectronics*, *22*, 3120–3125.

Liu, Z., Robinson, J. T., Sun, X., & Dai, H. (2008). PEGylated Nanographene Oxide for Delivery of Water-Insoluble Cancer Drugs. *J. Am. Chem. Soc.*, *130*, 10876–10877.

Lomocso, T. L., & Baranova, E. A. (2011). Electrochimica Acta Electrochemical oxidation of ammonia on carbon-supported bi-metallic PtM ( M = Ir , Pd , SnO x ) nanoparticles. *Electrochimica Acta*, *56*(24), 8551–8558.

Lu, L., Zhang, O., Xu, J., Wen, Y., Duan, X., & Yu, H. (2013). Sensors and Actuators B : Chemical A facile one-step redox route for the synthesis of graphene / poly ( 3 , 4-ethylenedioxythiophene ) nanocomposite and their applications in biosensing. *Sensors & Actuators: B. Chemical*, *181*, 567–574. https://doi.org/10.1016/j.snb.2013.02.024

Ma, F.-X., Wang, J., Wang, F.-B., & Xia, X.-H. (2015). The room temperature electrochemical synthesis of N-doped graphene and its electrocatalytic activity for oxygen reduction. *Chem. Commun.*, *51*(7), 1198–1201.

Mani, V., Periasamy, A. P., & Chen, S. (2012). Electrochemistry Communications Highly selective amperometric nitrite sensor based on chemically reduced graphene oxide modi fi ed electrode. *Electrochemistry Communications*, *17*, 75–78.

Marcano, D. C., Kosynkin, D. V, Berlin, J. M., Sinitskii, A., Sun, Z., Slesarev, A., … Tour, J. M. (2010). Improved Synthesis of Graphene Oxide. *ACS Nano*, *4*(8).

Nioradze, N., Chen, R., Kurapati, N., Khvataeva-domanov, A., & Amemiya, S. (2015). Organic Contamination of Highly Oriented Pyrolytic Graphite As Studied by Scanning Electrochemical Microscopy. *Analytical Biochemistry*, *87*, 4836–4843.

Novoselov, K. S., & Geim, A. K. (2004). Electric Field Effect in Atomically Thin Carbon Films. *Science*, *306*(October), 666–670.

Österholm, A., Lindfors, T., Kauppila, J., Damlin, P., & Kvarnström, C. (2012). Electrochimica Acta Electrochemical incorporation of graphene oxide into conducting polymer films. *Electrochimica Acta*, *83*, 463–470.

Park, S., & Ruoff, R. S. (2009). Chemical methods for the production of graphenes. *Nature Nanotechnology*, *4*(4), 217–224.

Peterson, A. W., Heaton, R. J., & Georgiadis, R. M. (2001). The effect of surface probe density on DNA hybridization. *Nucleic Acids Research*, *29*(24), 5163–5168.

Qu, L., Liu, Y., Baek, J., & Ḱ, L. D. (2010). Nitrogen-Doped Graphene as Efficient Metal-Free Electrocatalyst for Oxygen Reduction in Fuel Cells. *ACS Nano*, *4*(3), 1321–1326.

Rafiee, J., Song, H., Yu, Z.-Z., Srivastava, I., Rafiee, M. A., Wang, Z., & Koratkar, N. (2009). Fracture and Fatigue in Graphene Nanocomposites. *Small*, *6*(2), 179–183.

Schniepp, H. C., Li, J. L., McAllister, M. J., Sai, H., Herrera-Alonson, M., Adamson, D. H., … Aksay, I. A. (2006). Functionalized single graphene sheets derived from splitting graphite oxide. *Journal of Physical Chemistry B*, *110*(17), 8535–8539.

Seredych, M., Hulicova-jurcakova, D., Qing, G., & Bandosz, T. J. (2008). Surface functional groups of carbons and the effects of their chemical character , density and accessibility to ions on electrochemical performance. *Carbon*, *46*, 1475–1488.

Shao, Y., Wang, J., Engelhard, M., Wang, C., & Lin, Y. (2010). Facile and controllable electrochemical reduction of graphene oxide and its applications †. *Journal of Materials Chemistry*, *20*, 743–748.

Shao, Y., Wang, J., Wu, H., Liu, J., Aksay, I. A., & Lin, Y. (2010). Graphene Based Electrochemical Sensors and Biosensors : A Review. *Electroanalysis*, *22*(10), 1027–1036.

Shao, Y., Zhang, S., Engelhard, M. H., Li, G., Shao, G., Wang, Y., … Lin, Y. (2010). Nitrogen-doped graphene and its electrochemical applications. *Journal of Materials Chemistry*, *20*(35), 7491–7496.

Stackelberg, M. V., Pilgram, M., & Toome, V. (1953). Bestimmung von Diffusionskoeffizienten einiger Ionen in wäßriger Lösung in Gegenwart von Fremdelektrolyten. *Elektrochemie*, *57*(5), 342–353.

Stankovich, S., Dikin, D. A., Piner, R. D., Kohlhaas, K. A., Kleinhammes, A., Jia, Y., … Ruoff, R. S. (2007). Synthesis of graphene-based nanosheets via chemical reduction of exfoliated graphite oxide. *Carbon*, *45*(7), 1558–1565.

Sundramoorthy, A. K., Vignesh Kumar, T. H., & Gunasekaran, S. (2018). *Chapter 12 - Graphene-Based Nanosensors and Smart Food Packaging Systems for Food Safety and Quality Monitoring A2 - Tiwari, Ashutosh BT - Graphene Bioelectronics*. *Advanced Nanomaterials*. Elsevier Inc.

Thermo Scientific. (2012). *Crosslinking Technical Handbook. Thermo Fisher Scientific*.

Torrisi, F., Hasan, T., Wu, W., Sun, Z., Lombardo, A., Kulmala, T. S., … Ferrari, A. C. (2012). Inkjet-printed graphene electronics. *ACS Nano*.

Turner, A. P. F., Karube, I., & Wilson, G. S. (1987). *Biosensors, fundamentals and applications.* Oxford: Oxford University Press.

Wang, Y., Shao, Y., Matson, D. W., Li, J., & Lin, Y. (2010). Nitrogen-Doped Graphene and Its Biosensing. *ACS Nano*, *4*(4), 1790–1798.

Wei, D., Liu, Y., Wang, Y., Zhang, H., Huang, L., & Yu, G. (2009). Synthesis of N-doped graphene by chemical vapor deposition and its electrical properties., Nano Lett. *Nano Letters*, *9*(5), 1752–1758.

Wei, D., & Liu, Y. (2010). Controllable synthesis of graphene and its applications. *Advanced Materials*, *22*(30), 3225–3241.

Yamaguchi, H., Granstrom, J., Nie, W., Sojoudi, H., Fujita, T., Voiry, D., … Graham, S. (2014). Reduced Graphene Oxide Thin Films as Ultrabarriers for Organic Electronics. *Advanced Energy Materials*, 4–9

Yang, Y., Shi, W., Zhang, R., Luan, C., Zeng, Q., Wang, C., … Ji, X. (2016). Electrochemical Exfoliation of Graphite into Nitrogen-doped Graphene in Glycine Solution and its Energy Storage Properties. *Electrochimica Acta*, *204*, 100–107.

Yu, H. Z., Luo, C. Y., Sankar, C. G., & Sen, D. (2003). Voltammetric procedure for examining DNA-modified surfaces: Quantitation, cationic binding activity, and electron-transfer kinetics. *Analytical Chemistry*, *75*(15), 3902–3907.

Zhang, L., & Xia, Z. (2011). Mechanisms of oxygen reduction reaction on nitrogen-doped graphene for fuel cells. *Journal of Physical Chemistry C*, *115*(22), 11170–11176.

Zhang, X., Zhang, D., Chen, Y., Sun, X., & Ma, Y. (2012). Electrochemical reduction of graphene oxide films: Preparation, characterization and their electrochemical properties. *Chinese Science Bulletin*, *57*(23), 3045–3050.

Zhou, M., Wang, Y., Zhai, Y., Zhai, J., Ren, W., Wang, F., & Dong, S. (2009). Controlled synthesis of large-area and patterned electrochemically reduced graphene oxide films. *Chemistry - A European Journal*, *15*(25), 6116–6120.

Zhu, Y., Sun, Z., Yan, Z., Jin, Z., & Tour, J. M. (2011). Rational design of hybrid graphene films for high-performance transparent electrodes. *ACS Nano*, *5*(8), 6472–6479.

# 8. Summary in Swedish – Svensk sammanfattning

## Elektrokemisk reduktion och samtidig N-dopning av nanografenoxid i acetonitril för DNA-selektiva biosensorer

När det gäller medicinsk diagnostik är det viktigt att snabbt och pålitligt upptäcka närvaron av en analyt inom ett prov. Detta kan göras med biosensorer som är modifierade med en biomolekyl som med hög selektivitet kan detektera analyten. Till exempel använder ett hemgranskningstest den starka affiniteten hos en antikropp för dess antigen, i det här fallet hormonet hCG som är närvarande i urinen hus en gravid kvinna, för att upptäcka graviditet. När urinprovet kommer i kontakt med testremsan binds enzymmodifierade antikroppar selektivt till hCG, som i sin tur binder till antikroppar som är immobiliserade på testremsan. Denna process resulterar i en färgförändring som kan ses som en positiv linje i testet. På liknande sätt kan en specifik DNA-sekvens detekteras inom ett prov genom att utnyttja det faktum att DNA är framställt av två enkla strängar som är bundna tillsammans av deras komplementära baspar och som bildar dubbelsträngat DNA. Detekteringen av en specifik DNA-sträng kan vara ovärderlig för diagnosen av genetiska sjukdomar och förstadier av cancer. Generellt görs DNA-sekvensering genom speciella sekvenseringsinstrument som bestämmer ordningen för baspar i en DNA-sträng. Enkelsträngat DNA som är immobiliserat på elektrodytan, definierad som DNA-sonden, binder till komplementärt DNA (kDNA), som är närvarande i provet. Den har bindningen, som är definierad som hybridisering, förändrar den elektriska signalen och medför en positiv signal som erhållas snabbt elektrokemiskt. Kraven för en sådan teknik är att DNA-biosensorn har hög selektivitet för en specifik DNA-sekvens, för att undvika ett falskt positivt svar, och en hög känslighet, för att detektera de mycket små koncentrationerna av DNA som är närvarande i provet.

Denna magisteruppsats fokuserar på modifieringsproceduren och utformningen av en DNA-biosensor som kan selektera kDNA och mata ut en detekterbar elektrisk signal. Sensorn är byggd som en serie byggstenar, där var och en är en nyckelkomponent i sensorns övergripande funktion. En glasaktig kolstav används som elektrodmaterial eftersom den är inert och ger bra elektronöverföringsförmåga. För att erhålla den förstärkta elektriska signalen modifieras elektrodytan med ett material som härrör från grafen. Grafen har i sig varit ett fokus för forskning i ett antal år på grund av dess ökade ytarea och elektriska ledningsförmåga, vilket gör det till en valid kandidat för elektrokemisk avkänning. På grund av dess begränsningar i massproduktion används ren grafen sällan, men istället kan derivaten av grafen modifieras för att nå liknande elektriska egenskaper. Grafenoxid (GO) som är en grafenderivat är en isolator men kan reduceras för att avlägsna de syreinnehållande grupperna som ger den sina isolerande egenskaper, och därmed återställs dess

elektriska ledningsförmåga. För att ytterligare öka materialledningsförmågan kan ett störämne introduceras till grafenoxiden, som antingen tillhandahåller elektroner som en elektrondonator eller ett hål som en elektronacceptor. Kvävet är effektivt som elektrondonator och används ofta som störämne i grafenoxidförstärkningen av dess elektrokatalytiska egenskaper. Dessutom möjliggör kvävehaltiga grupper som införs i grafenkonstruktionen ytterligare modifiering av ytan med DNA-sonden genom tvärbindningskemi. En tvärbindare har förmågan att reagera med specifika funktionella grupper som bildar kovalenta bindningar. I detta fall kan den ena ändan av tvärbindaren binda till kvävehaltiga grupper inom den reducerade och N-dopade grafenoxiden (RNGO), medan den andra ändan binder till ändan av DNA-sonden som är kemiskt modifierad med en merkaptogrupp. När DNA-sonden är tvärbunden till NRGO-ytan kan endast komplementärt eller delvis komplementärt DNA hybridisera med sonden. Framgångsrik hybridisering detekteras genom att utföra cyklisk voltametri i en bärande elektrolyt som innehåller en redox-katjon, såsom $[Ru(NH_3)_6]^{3+}$, som elektrostatiskt binder till DNA-strängarna och ger ett voltametriskt svar som motsvarar mängden DNA som är närvarande på ytan.

Ursprungligen kunde denna metod inte reproduceras inom den initiala gjutningen av GO, vilket orsakade ofullständig täckning av elektrodytan som påverkade följande steg negativt. En optimerad dropcasting-procedur utvecklades, och det bestämdes därför att gjutning av sjutton alikvoter á 5 µL GO-lösning och värmning i 1 timme vid 60 ° C gav den bästa yttäckningen (figur 4). Följande steg, reduktion och N-dopning av GO, optimerades också för att nå den högsta framgångsrika selektiviteten hos elektroderna för kDNA. Med tanke på att DNA-sonden är immobiliserad på ytan via de kväveinnehållande grupperna, har omfattningen av reduktion och N-dopning en direkt effekt på sensorns prestation. En större grad av N-dopning skulle leda till en större densitet av DNA-sonden på elektrodytan, men vid en för hög densitet är elektrodytan för trång och hämmar hybridiseringen av kDNA. Potentialens räckvidd, och därmed omfattningen av reduktion och graden av N-dopning, varierades för att bestämma de optimala betingelserna för kDNA-detektion (tabell 1). Det resulterande materialet visade en förbättrad reproducerbarhet såväl som en förstärkt strömsignal jämfört med den tidigare sensordesignen (figur 8). Det optimerade materialet karakteriserades med användning av analytiska tekniker såsom cyklisk voltametri och elektrokemisk impedansspektroskopi för att bättre förstå dess elektrokemiska egenskaper. N-dopning resulterade i en negativt laddad yta men ökade också materialets elektriska konduktivitet (figur 10). Vid tillämpning av en DNA-biosensor ökade materialet hastigheten för framgångsrik kDNA-hybridisering till 100 % och amplifierade responsen 1,5 gånger (figur 17). Det pågående arbetet lyckades därför med att förbättra metoderna för att förbereda reducerad och N-dopad GO med en direkt applicering i en DNA-selektiv biosensor.